Title

NMNAT1 facilitates energy metabolism and gene regulation in developing retinal neurons

Authors

David Sokolov[1]

Emily Sechrest[1,2]

Yekai Wang[2,3]

Connor Nevin[1]

Jianhai Du[1,3]

Saravanan Kolandaivelu[1,3,*]

Affiliations

[1]Department of Ophthalmology and Visual Sciences, Eye Institute, One Medical Center Drive, West Virginia University, Morgantown, WV, 26506-9193, USA

[2]Department of Pharmaceutical Sciences, One Medical Center Drive, West Virginia University, Morgantown, WV, 26506-9193, USA

[3]Department of Biochemistry, One Medical Center Drive, West Virginia University, Morgantown, WV, 26506-9193, USA

*Corresponding Author, kolandaivelus@hsc.wvu.edu

ABSTRACT

Despite mounting evidence that the mammalian retina is exceptionally reliant on proper NAD^+ homeostasis for health and function, the specific roles of subcellular NAD^+ pools in retinal development, maintenance, and disease remain obscure. Here, we show that deletion of the nuclear-localized NAD^+ synthase nicotinamide mononucleotide adenylyltransferase-1 (NMNAT1) in the developing murine retina causes early and severe degeneration of photoreceptors and select inner retinal neurons via multiple distinct cell death pathways. This severe phenotype is associated with extra-nuclear metabolic disruptions to retinal central carbon metabolism, purine nucleotide synthesis, and amino acid pathways. Furthermore, large-scale transcriptomics reveals dysregulation of a collection of photoreceptor and synapse-specific genes in NMNAT1 knockout retinas prior to detectable morphological or metabolic alterations. Collectively, our study furthers understanding of subcellular NAD^+ metabolism in vision, reveals previously unrecognized complexity in NMNAT1-associated retinal degeneration, and suggests a yet-undescribed role for NMNAT1 in genetic regulation of photoreceptor terminal differentiation.

46

47 **INTRODUCTION**

48

49 Nicotinamide adenine dinucleotide (NAD^+) is a ubiquitous cellular metabolite with an ever-
50 expanding palette of biological functions across all kingdoms of life. In addition to serving a
51 central role in redox metabolism as an electron shuttle, NAD^+ has well-defined roles as a
52 substrate for a host of enzymes including sirtuins (SIRTs), mono- and poly- ADP-ribose
53 polymerases (PARPs), and glycohydrolases (CD38, CD157, and SARM1), whose collective
54 functions implicate NAD^+ metabolism in phenomena as diverse as aging, cell proliferation,
55 immunity, neurodegeneration, differentiation, and development (Houtkooper et al., 2010; Canto
56 et al., 2015; Nikiforov et al., 2015; Cambronne and Kraus, 2020; Navas and Carnero, 2021). A
57 relatively recent advance in the field is the notion of compartmentalized NAD^+ metabolism—that
58 production, utilization, and regulation of NAD^+ in distinct subcellular compartments dictates
59 function in tissue and process specific manners (Canto et al., 2015; Nikiforov et al., 2015;
60 Cambronne and Kraus, 2020; Navas and Carnero, 2021). While many aspects of this
61 compartmentalization remain to be explored, it is now known that spatiotemporal NAD^+
62 regulation plays prominent roles in processes including axon degeneration, circadian regulation,
63 and adipogenesis (Cambronne and Kraus, 2020).

64

65 Among mammalian tissues, the retina appears particularly reliant on proper NAD^+ homeostasis
66 for survival and function. This is evidenced first and foremost by over 30 mutations to the
67 ubiquitous, nuclear-localized NAD^+-synthesizing enzyme NMNAT1 which cause the severe
68 blinding disease Leber congenital amaurosis type 9 (LCA9) and related cone dystrophy (Perrault

69 et al., 2012; Falk et al., 2012; Chiang et al., 2012; Koenekoop et al., 2012; Coppieters et al.,
70 2015; Nash et al., 2018). Although many of these mutations reduce NMNAT1 catalytic activity
71 or stress-associated stability (Falk et al., 2012; Koenekoop et al., 2012; Sasaki et al., 2015),
72 patients with these disorders rarely report extra-ocular phenotypes, and two NMNAT1 mutant
73 mouse models recapitulate this puzzling observation (Greenwald et al., 2016). Further supporting
74 the importance of NAD^+ metabolism to vision are associations between retinal NAD^+ deficiency
75 and pathology in diverse models of retinal dysfunction (Lin et al., 2016) as well as multiple
76 mutations to NAD^+- or $NADP^+$-utilizing enzymes which also cause blindness in humans (Bowne
77 et al., 2006; Aleman et al., 2018; Bennett et al., 2020). Indeed, a crucial role for retinal NAD^+
78 was recently described through characterization mice conditionally lacking the rate-limiting
79 NAD^+ pathway enzyme NAMPT in photoreceptors (Lin et al., 2016). While Lin et al. shed light
80 on potential links between NAD^+ and mitochondrial metabolism in photoreceptors, the
81 significance of compartmentalized NAD^+ in vision—suggested by the fact that NMNAT1 is the
82 only NAD^+-pathway enzyme to date linked to blindness—remains poorly understood.
83
84 In mammals, NAD^+ is synthesized through four principal routes: *de novo* from tryptophan, from
85 diet-supplied nicotinic acid (NA) or nicotinamide riboside (NR), or from nicotinamide (NAM).
86 The final step of NAD^+ synthesis—common to all four pathways—is catalyzed by members of
87 the nicotinamide mononucleotide adenylyltransferase (NMNAT) family, which transfer an
88 adenylyl group from ATP to nicotinamide mononucleotide (NMN) or nicotinic acid
89 mononucleotide (NaMN) to form NAD^+ (Nikiforov et al., 2015). There are three NMNAT
90 isoforms in mammals (NMNAT1, 2, and 3) which differ in relative expression, activity, and
91 subcellular localization and maintain organelle-specific NAD^+ pools under various conditions

92 (Mori et al., 2014; Cambronne and Kraus, 2020). Among these isoforms, NMNAT1 and
93 NMNAT2 show relatively high gene expression in the retina (Kuribayashi et al., 2018) and
94 NMNAT1, which is localized to the cell nucleus, has gained considerable attention due to the
95 aforementioned links to disease as well as described roles in neuroprotection (Brazill et al.,
96 2017).
97
98 Current results point to multiple, potentially distinct roles for NMNAT1 in the mammalian
99 retina—*ex vivo* studies suggest that NMNAT1 supports retinal sirtuin function to facilitate the
100 survival of retinal progenitors (Kuribayashi et al., 2018), while ablation of NMNAT1 in mature
101 mice results in rapid death of photoreceptors mediated by the neurodegenerative NAD^+
102 glycohydrolase SARM1 (Sasaki et al., 2020a). Global deletion of NMNAT1 in mice is
103 embryonically lethal (Conforti et al., 2011), suggesting non-redundant roles for nuclear NAD^+
104 synthesis during development. Consistent with this notion, pan-retinal NMNAT1 deletion is
105 shown to cause rapid and severe retinal degeneration in mice shortly after birth (Wang et al.,
106 2017; Eblimit et al., 2018). While these studies suggest diverse functions of retinal NMNAT1
107 beyond its canonical role in redox metabolism, the degree to which these functions overlap—as
108 well as the mechanistic basis for the severity of NMNAT1-associated retinal dystrophy in animal
109 models and patients—have not been comprehensively explored.
110
111 In this study, we investigate the roles of NMNAT1-mediated NAD^+ metabolism in the retina by
112 generating and characterizing a retina-specific NMNAT1 knockout mouse model. Utilizing
113 histological and transcriptomic approaches, we demonstrate that NMNAT1 deletion causes
114 severe and progressive retinal degeneration affecting specific retinal cell types beyond

115 photoreceptors, and that this severe degeneration likely results from activation of multiple
116 distinct cell death pathways. Comprehensive metabolomics analysis reveals extra-nuclear
117 metabolic defects in NMNAT1 knockout retinas and suggests impaired central carbon, purine
118 nucleotide, and amino acid metabolism as a cause for severe degeneration. Unexpectedly,
119 transcriptomics analyses of knockout retinas reveal a cluster of photoreceptor and synapse-
120 specific genes which are downregulated before the onset of degeneration, suggesting a yet-
121 undescribed role for NMNAT1 in gene regulation during late-stage retinal development. Overall,
122 our results reveal a previously unappreciated complexity in NMNAT1-associated retinal
123 degeneration, provide possible explanations for the retina-specific manifestations of NMNAT1
124 deficiency, and lay the foundation for further study of compartmentalized NAD^+ metabolism in
125 vision.
126
127 **RESULTS**
128
129 **Generation and validation of NMNAT1 conditional knockout mouse model**
130 To establish a retinal-specific NMNAT1 knockout model, we crossed transgenic mice
131 homozygous for a loxP-targeted *Nmnat1* locus (*Nmnat1*$^{fl/fl}$) with mice expressing Cre
132 recombinase under a *Six3* promoter (*Nmnat1*$^{wt/wt}$ *Six3-Cre*), which activates throughout the retina
133 around embryonic day 9.5 (E9.5) and shows robust activity by E12.5 (Furuta et al., 2000). After
134 several crosses, mice inheriting *Six3-Cre* and a targeted *Nmnat1* locus (*Nmnat1*$^{fl/fl}$ *Six3-Cre*,
135 hereafter referred to as "knockouts") exhibit Cre-mediated excision of the first two exons of
136 *Nmnat1*—which contain important substrate binding domains—in the embryonic retina (**Figure**
137 **1A**). We determined that retinal *Nmnat1* expression in postnatal day 4 (P4) knockout mice was

138 reduced by 75.6% compared to littermate controls (**Figure 1B**). We further verified that retinal
139 NMNAT1 protein levels were drastically reduced in P0 knockout mice using a custom-made
140 polyclonal antibody against NMNAT1 (**Figure 1C** and **Figure 1—Supplement 1**). Finally, we
141 confirmed that embryonic *Six3-Cre* expression alone does not cause gross retinal abnormalities
142 by staining for several well-characterized cell type markers in mature *Nmnat1*$^{wt/wt}$ *Six3-Cre*
143 retinas and littermate controls (**Figure 2—Supplement 1**; markers discussed below).

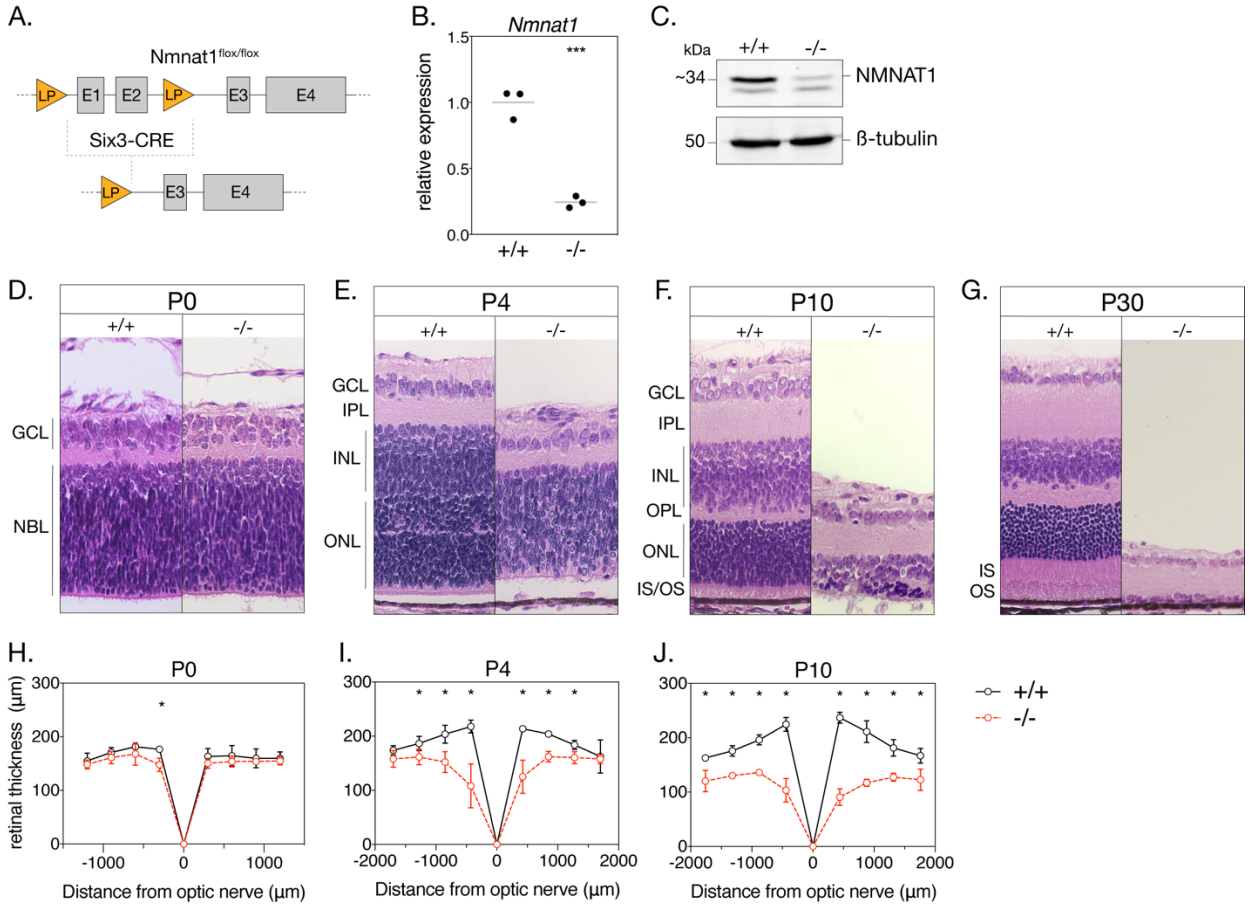

144

145 **Figure 1. Loss of NMNAT1 leads to early and severe retinal degeneration.** (**A**) schematic
146 depicting retina specific *Six3-Cre* mediated excision of a segment of the *Nmnat1* gene. (**B**)
147 relative *Nmnat1* expression in retina from P4 knockout (-/-) and littermate control (+/+) mice as
148 assessed by RT-qPCR (grey bars represent mean, ***p<0.0005 using Student's t-test, n=3
149 biological replicates). (**C**) representative western blot showing levels of NMNAT1 and β-tubulin
150 loading control in retinal lysate from P0 knockout and control mice. (**D-G**) representative
151 hematoxylin and eosin (H&E)-stained retinal cross sections from knockout and control mice at
152 indicated ages. (**H-J**) spider plots depicting mean retinal thickness at P0, P4, and P10. Data are
153 represented as mean ± SD. *p<0.05 using Student's t-test. Abbreviations: LP, loxP site; E1-4,

154 exon 1-4; P, postnatal day; GCL, ganglion cell layer; NBL, neuroblastic layer; IPL, inner
155 plexiform layer; OPL, outer plexiform layer; INL, inner nuclear layer; ONL, outer nuclear layer;
156 IS/OS, photoreceptor inner segment/outer segment layer.
157
158
159
160
161 **Early-onset and severe morphological defects in the NMNAT1-null retina**
162
163 As a first step towards characterizing the effects of NMNAT1 ablation on the retina, we
164 performed retinal histology using hematoxylin and eosin (H&E) staining. H&E-stained retinal
165 cross sections from P0 knockout and control mice reveal no obvious morphological differences
166 (**Figure 1D,H**); however, by P4, knockout retina are markedly thinner than controls and exhibit
167 disrupted lamination and evidence of large-scale cell death in the inner and outer nuclear layers
168 (**Figure 1E**). Degeneration is most severe in the central retina, with a ~45% reduction in central
169 retinal thickness (but unaffected peripheral retinal thickness) in P4 knockout mice (**Figure 1I**).
170 By P10, knockouts show a ~62% reduction in central retinal thickness and ~27% reduction in
171 peripheral retinal thickness compared to controls (**Figure 1J**). Degeneration of the entire inner
172 and outer nuclear layers is nearly complete by P30 (**Figure 1G**), while remaining inner retinal
173 structures persist until approximately P60 (data not shown). Proper segregation of inner and
174 outer retinal neurons appears disrupted in P4 knockouts, but this segregation is established in
175 P10 knockouts despite severe degeneration (**Figure 1F**). Interestingly, formation of the outer
176 plexiform layer (containing photoreceptor and bipolar neuron synaptic structures) appears
177 disrupted in P4 and P10 knockout retinas (**Figure 1E,F**).
178
179 **NMNAT1 loss affects survival of retinal bipolar and amacrine neurons**
180 Histological examination suggests severe photoreceptor degeneration in NMNAT1 knockout
181 retinas but also indicates loss of specific inner retinal neuron populations. To further characterize

182 these effects, we quantified populations of several major inner retinal cell types in our knockout
183 by staining retinal sections with well-characterized antibody markers of retinal ganglion cells
184 (anti-BRN3A), amacrine cells (anti-calretinin), and bipolar cells (anti-CHX10) (**Supplemental**
185 **Table 2**). We performed this analysis at P4 and P10—representing early and late stages of
186 degeneration, respectively—revealing an interesting cell type-dependent sensitivity to NMNAT1
187 loss (**Figure 2**). At both tested ages, relative numbers of BRN3A-positive retinal ganglion cells
188 are not significantly different between knockout and control retina (**Figure 2B-E, P**), while
189 numbers of calretinin-positive amacrine cells are unchanged at P4 but reduced by ~51% in P10
190 knockout retinas (**Figure 2G-J, Q**). Numbers of CHX10-positive bipolar cells are similarly
191 unchanged at P4 but reduced by ~75% in P10 knockout retinas (**Figure 2L-O, R**). These results
192 identify retinal bipolar and amacrine neurons as targets of NMNAT1-associated degeneration
193 and suggest that bipolar neurons are more sensitive to NMNAT1 loss than amacrine neurons.
194 Interestingly, while BRN3A-positive retinal ganglion cells do eventually degenerate at
195 timepoints past P30 (data not shown), they appear largely agnostic to NMNAT1 loss in the
196 young postnatal retina.

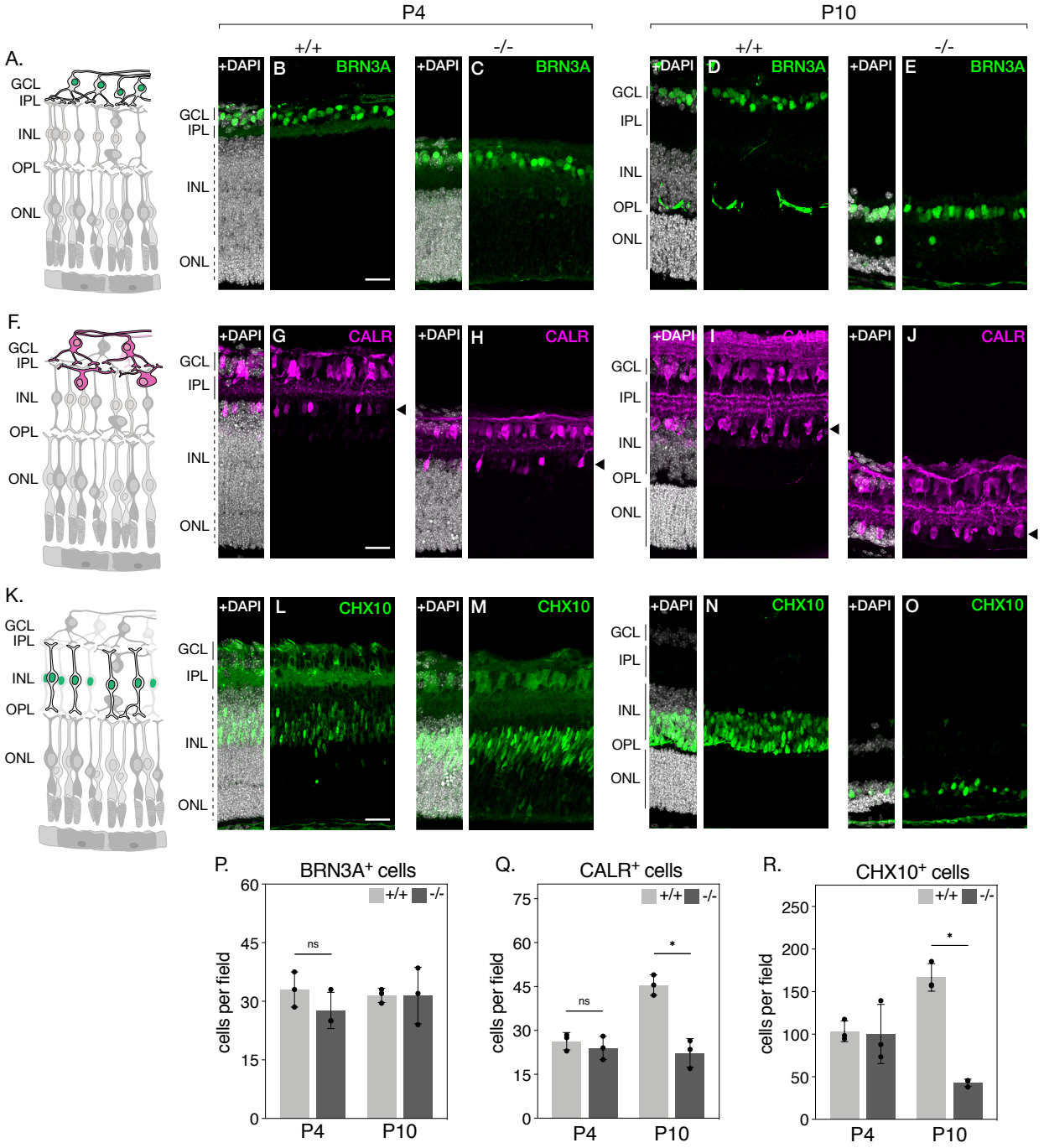

Figure 2. NMNAT1 loss affects survival of retinal bipolar and amacrine cells. Representative retinal sections from knockout (-/-) and floxed littermate control (+/+) mice at the indicated ages labelled with antibodies against BRN3A (**B-E***)*, Calretinin (CALR) (**G-J***)*, and CHX10 (**L-O***)*. Schematics in (**A**), (**F**), and (**K**) depict retinal neuron subtypes labelled by each respective antibody. Quantification of BRN3A- (**P***)*, Calretinin- (**Q***)*, and CHX10-positive cells (**R**) are shown. In (**Q**), only calretinin-positive cells on the outer side of the IPL (layer indicated by arrowheads) were counted. Data is represented as mean ± SD. n=3 biological replicates for all panels; significance determined using Student's t-test. Scale bars, 30 μm.

207 **Loss of NMNAT1 impairs photoreceptor gene expression and severely perturbs early**
208 **postnatal photoreceptor survival**
209 Turning our attention to photoreceptors, we repeated the above approach with antibodies against
210 the photoreceptor markers recoverin (anti-RCVRN) and rhodopsin (anti-RHO). While anti-
211 RCVRN cleanly labels developing photoreceptor somas in P4 and P10 control retinas (**Figure**
212 **3B, Figure 3—Supplement 1, panel D**), we observe a complete lack of recoverin staining in
213 knockout retinas at both ages (**Figure 3C, Figure 3—Supplement 1, panel E).** Barring a small
214 amount of non-specific staining likely originating from the secondary antibody (**Figure 3—**
215 **Supplement 1, panels A,B**), rhodopsin staining at P4 and P10 showed an identical trend to that
216 of recoverin (**Figure 3D,E, Figure 3—Supplement 1, panels H,I**).
217
218 Intrigued by the magnitude of this effect, and hypothesizing a role for NMNAT1-synthesized
219 nuclear NAD^+ in retinal gene regulation, we comprehensively profiled the transcriptomes of
220 knockout and control retinas at two timepoints—during degeneration (P4) and pre-degeneration
221 (E18.5)—using RNA-sequencing. At P4, this analysis reveals 2,976 differentially-expressed
222 genes in NMNAT1 knockout retinas (**Figure 3—Supplement 2, panel B**), several of which we
223 validated using RT-qPCR (**Figure 3—Supplement 1, panel C**). Consistent with the lack of
224 recoverin and rhodopsin staining at this age, gene set enrichment analysis (GSEA) of P4
225 differentially-expressed genes reveals several large, highly-overrepresented clusters of
226 downregulated genes associated with phototransduction and the cilium, including both recoverin
227 and rhodopsin (**Figure 3—Supplement 2, panel C**). Strikingly, among 815 differentially-
228 expressed genes in E18.5 knockout retinas, a similar cluster of downregulated genes associated
229 with visual perception and the photoreceptor outer segment was observed (**Figure 3—**

230 **Supplement 3, panels B, C**). Combining both RNA-sequencing datasets reveals a group of 365
231 genes which are differentially expressed in knockout retinas at both timepoints (**Figure 3F**).
232 Importantly, GSEA on this gene set reveals highly-overrepresented clusters of photoreceptor and
233 synapse associated genes (**Figure 3G**), and further analysis identifies a core set of 21
234 photoreceptor-associated genes which are significantly downregulated in E18.5 and P4
235 NMNAT1 knockout retinas (**Figure 3H,I**). Notably, this set includes rod-specific (e.g. *Gngt1*),
236 cone-specific (e.g. *Opn1sw*, *Cnga3*) and photoreceptor-specific (e.g. *Prph2*, *Rcvrn*, *Aipl1*) genes
237 of diverse function, many of which have important roles in photoreceptor development and
238 function. Consistent with a specific transcriptional effect on photoreceptors, we confirmed that
239 expression of several well-known ganglion cell, amacrine/horizontal cell, and bipolar cell
240 specific genes was largely unchanged in NMNAT1 knockout retinas at either tested age (**Figure**
241 **3—Supplement 4**). Altogether, these results implicate NMNAT1 in gene regulation during late-
242 stage retinal development, and suggest predominantly photoreceptor-specific transcriptional
243 dysregulation as a driver of the severe photoreceptor phenotype in NMNAT1 deficient retinas.
244
245 Beyond affecting photoreceptor-specific gene expression, we also note downregulation of 6
246 synapse-associated genes (*Stx3*, *Syngr1*, *Cln3*, *Scamp5*, and *Sv2b*) in both E18.5 and P4 knockout
247 retinas (**Figure 3—Supplement 5, panels C,D**), consistent with disruptions to outer plexiform
248 layer formation in P4 knockout retinas on histology and on staining with the synapse marker
249 synaptophysin (anti-SYPH) (**Figure 3—Supplement 5**).

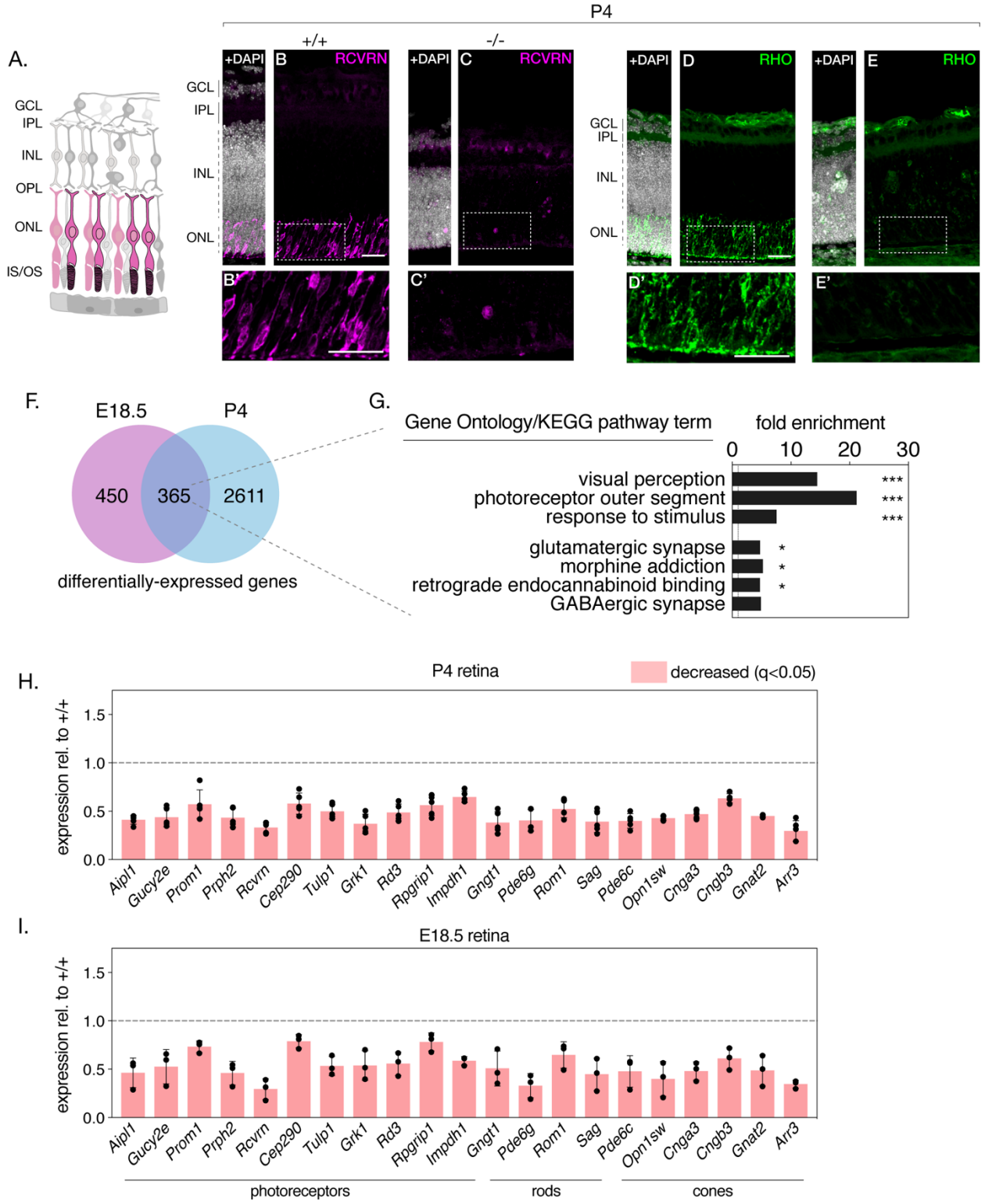
A.
P4
+/+
-/-
GCL
IPL
INL
OPL
ONL
IS/OS
+DAPI
B
RCVRN
C
D
RHO
E
B'
C'
D'
E'
F.
E18.5
P4
450
365
2611
differentially-expressed genes
G.
Gene Ontology/KEGG pathway term
fold enrichment
0
10
20
30
visual perception
photoreceptor outer segment
response to stimulus
glutamatergic synapse
morphine addiction
retrograde endocannabinoid binding
GABAergic synapse
***
*
H.
P4 retina
decreased (q<0.05)
expression rel. to +/+
1.5
1.0
0.5
0.0
Aipl1
Gucy2e
Prom1
Prph2
Rcvrn
Cep290
Tulp1
Grk1
Rd3
Rpgrip1
Impdh1
Gngt1
Pde6g
Rom1
Sag
Pde6c
Opn1sw
Cnga3
Cngb3
Gnat2
Arr3
I.
E18.5 retina
photoreceptors
rods
cones

250
251
252

253 **Figure 3. NMNAT1 loss severely affects early postnatal photoreceptor gene expression and**
254 **survival.** Representative retinal sections from knockout (-/-) and floxed littermate control (+/+)
255 mice at the indicated ages labelled with antibodies against recoverin (RCVRN) (**B-C**) or
256 rhodopsin (RHO) (**D-E**). Schematic in (**A**) depicts retinal neuron subtypes labelled by recoverin
257 antibody. (**F**) comparison of differentially-expressed genes in E18.5 and P4 knockout retinas as
258 assessed by RNA-sequencing. (**G**) GSEA of differentially-expressed genes present in E18.5 and
259 P4 knockout retinas. (**H,I**) relative expression of indicated genes in P4 and E18.5 knockout
260 retinas as assessed by RNA-sequencing. n=3 biological replicates for (**B-E**), n=5 biological
261 replicates for (**H**), n=3 biological replicates for (**I**). Corresponding zoom panels are indicated
262 with dotted rectangles. Scale bars, 30 μm.
263

264 **Loss of NMNAT1 during retinal development triggers multiple cell death pathways**

265 As NMNAT1 deficiency drastically impairs the postnatal survival of photoreceptor, bipolar, and
266 amacrine neurons, we sought to determine the mechanisms by which these cells degenerate. To
267 this aim, we began by staining retinal sections with an antibody against activated caspase-3
268 (AC3). While P0 knockout retinas show little AC3 staining compared to controls—consistent
269 with grossly normal retinal morphology at this age—P4 knockout retinas show robust AC3
270 immunoreactivity in the inner and outer nuclear layers (**Figure 4A-D**). As expected, most AC3-
271 positive cells display nuclear chromatin condensation ('pyknosis') characteristic of dying cells;
272 however, staining also reveals a population of pyknotic nuclei not immunoreactive to AC3
273 (**Figure 4A'-D', arrows**). Interestingly, these pyknotic, AC3-negative cells were sparsely
274 present in P0 and P4 control retinas (**Figure 4A,C**) and to a larger extent in P0 and P4 knockout
275 retinas (**Figure 4B,D**). Quantification (**Figure 4E**) reveals a general trend of cell death consistent
276 with our histology and cell-marker investigations: nuclear pyknosis is slightly elevated in P0
277 knockout retinas compared to controls, peaks at P4 where we observe robust retinal
278 degeneration, and is virtually absent by P10, by which time the majority of outer and inner nuclei
279 in the knockout are lost (**Figure 1D**). Interestingly, we observe roughly equal amounts of AC3-
280 positive and AC3-negative pyknotic cells in P0 knockout retinas, whereas by P4 AC3-negative
281 pyknotic cells constitute ~30% of pyknotic cells in knockout retinas (**Figure 4E**). In addition to
282 being present at all tested ages and following the same general trend as AC3-
283

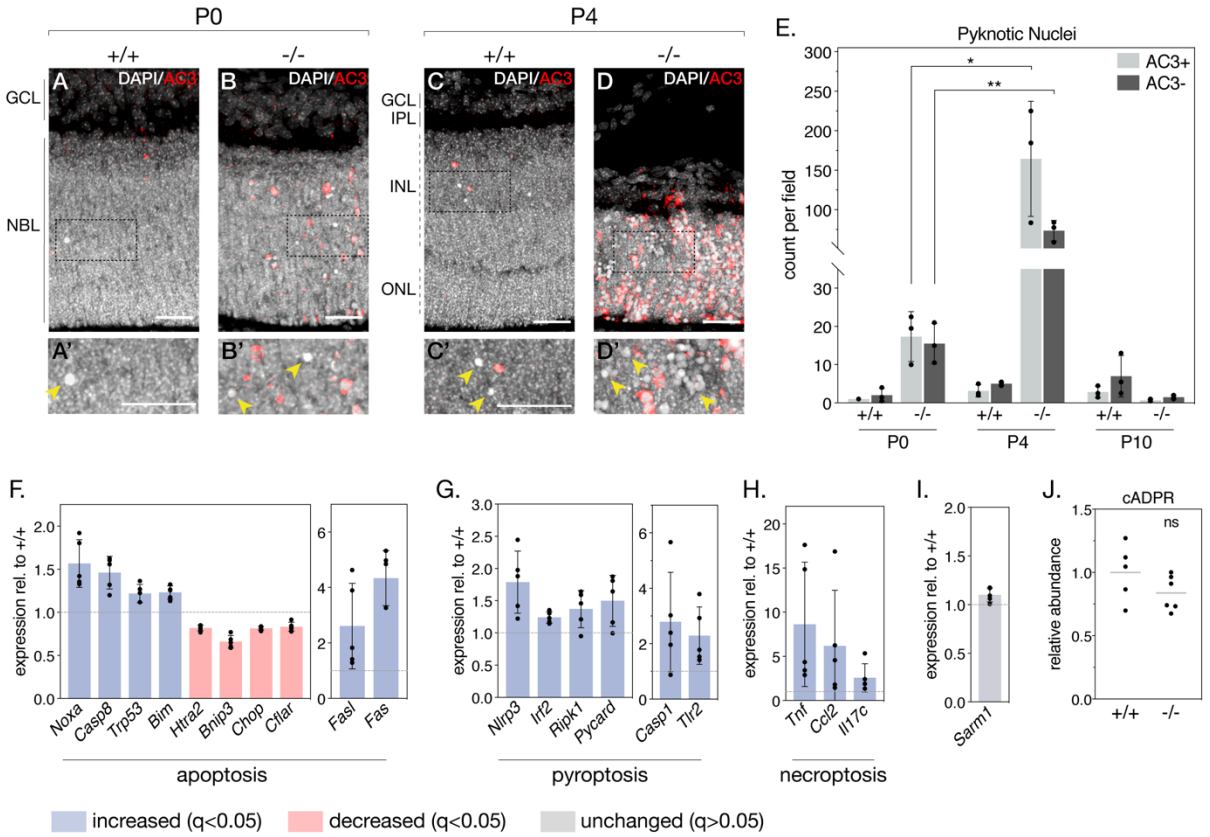

Figure 4. NMNAT1 loss causes activation of multiple cell death pathways in the retina. (A-D) representative retinal sections from knockout (-/-) and floxed littermate control (+/+) mice at the indicated ages labelled with an antibody against active Caspase-3 (AC3). Corresponding zoom panels are indicated with dotted rectangles. Arrows denote pyknotic, AC3-negative nuclei. **(E)** quantification of pyknotic nuclei in sections from knockout and control mice at the indicated ages, grouped by presence (AC3+) or absence (AC3-) of active Caspase-3 labeling. Relative expression of several apoptotic (**F**), pyroptotic (**G**), and necroptotic (**H**) genes in P4 knockout retinas as assessed by RNA-sequencing. **(I)** relative expression of *Sarm1* in P4 knockout and control retinas as assessed by RNA-sequencing. **(J)** relative abundance of cyclic-ADP-ribose (cADPR) in P4 knockout and control retinas as measured by mass spectrometry (grey bars represent means). Data are represented as mean ± SD. Significance determined using Tukey's multiple comparisons test for (**E**), DESeq2 for (**F-I**) (see methods), or Student's t-test for (**J**). n=3 biological replicates per condition for (**A-E**), n=5 biological replicates for (**F-I**), n=6 biological replicates (one outlier removed) for (**J**). Scale bars, 30 µm.

301
302 positive pyknotic cells, AC3-negative pyknotic cells often appear in distinct clusters (**Figure**
303 **4D'**), distinguishable from the more evenly dispersed AC3-positive pyknotic cells.
304
305 These results suggest the activation of at least two distinct cell death pathways in NMNAT1
306 knockout retinas between P0 and P4. To more comprehensively characterize NMNAT1-
307 associated cell death and identify possible caspase 3-independent cell death pathways in our
308 knockout, we leveraged the E18.5 and P4 RNA-sequencing datasets mentioned above. This
309 allowed us to systematically assay the expression of a collection of genes associated with several
310 major cell death pathways (**Figure 4—Supplement 2**). Consistent with AC3 staining, we
311 observe deregulation of a collection of apoptosis-related genes in P4 knockout retina, including
312 significant increases in *Noxa* and *Fas*, two pro-apoptotic genes previously associated with cell
313 death in NMNAT1-deficient retinas (Kuribayashi et al., 2018) (**Figure 4F**). Notably, two of
314 these genes—*Noxa* and *Chop*—are also significantly deregulated at E18.5, prior to significant
315 retinal degeneration (**Figure 4—Supplement 1, panel A**).
316
317 In addition to transcriptional signatures of apoptosis, we identified upregulation of a collection of
318 genes associated with pyroptosis in P4 NMNAT1 knockout retinas (**Figure 4G**). Pyroptosis is
319 characterized by assembly of a multi-protein complex called the 'inflammasome,' which
320 ultimately cleaves and activates the pore-forming members of the gasdermin family of proteins
321 to elicit lytic cell death in response to a variety of perturbations (McKenzie et al., 2020).
322 Interestingly, we find upregulation of all three classical inflammasome components—*Nlrp3*,
323 *Casp1*, and *Pycard* (ASC)—in P4 knockout retinas (**Figure 4G**), with *Nlrp3* upregulation at
324 E18.5 as well (**Figure 4—supplement 1, panel B**). In addition, we observe significant increases

325 in *Irf2*, a transcriptional activator of gasdermin D (Kayagaki et al., 2019), as well as pyroptosis-
326 associated proteins *Ripk1* and *Tlr2* at P4 (**Figure 4G**). Notably, expression of *Tlr2* and related
327 protein *Tlr4* is significantly elevated in E18.5 knockout retinas (**Figure 4—Supplement 1, panel**
328 **B**). Finally, we also observed dysregulation of several genes associated with necroptosis (**Figure**
329 **4H**) and ferroptosis (**Figure 4—Supplement 2, panel D**) in P4 knockout retinas; however, none
330 of these genes were significantly upregulated at E18.5, although we do observe an early
331 induction of necroptosis-associated protein *Nox2* at this age (**Figure 4—Supplement 1, panel**
332 **C**).
333
334 Recently, photoreceptor cell death in a postnatally-induced global NMNAT1 knockout mouse
335 was shown to depend heavily on the activity of the pro-degenerative axonal protein SARM1
336 (Sasaki et al., 2020a). Suspecting SARM1 as the culprit behind the caspase 3-independent cell
337 death in our model, we checked *Sarm1* expression in our RNA-seq data and assayed SARM1
338 activity by measuring levels of its catalytic product cyclic ADP-ribose (cADPR) using targeted
339 mass spectrometry in P4 and E18.5 NMNAT1 knockout and control retinas. Surprisingly, we
340 found no significant changes in SARM1 expression (**Figure 4I, Figure 4—Supplement 1, panel**
341 **D**) or activity (**Figure 4J, Figure 4—Supplement 1, panel E**) at either tested age. Overall, these
342 data reveal that activation of multiple cell death pathways underlies the rapid and severe
343 degeneration observed in NMNAT1 knockout retinas, and suggest pyroptosis—rather than
344 SARM1—and apoptosis as drivers of this degeneration.
345
346
347

348 **Global metabolic consequences of retinal NMNAT1 ablation**

349 To identify possible mechanisms for the severe and cell type-specific retinal degeneration in our
350 model, we sought to characterize global metabolic consequences of deleting NMNAT1 in the
351 retina. To this end, we used targeted liquid chromatography-tandem mass spectrometry (LC-
352 MS/MS) to quantify levels of ~112 cellular metabolites spanning many essential biochemical
353 pathways in NMNAT1 knockout and control retinas at pre- and post-degenerative timepoints
354 matching that of our RNA-sequencing analyses (E18.5 and P4). While LC-MS/MS analysis
355 reveals no significant changes in E18.5 knockout retinas compared to controls, analysis at P4
356 reveals significantly altered levels of 39 metabolites in knockout retinas (**Figure 5, Figure 5—**
357 **Supplement 1**). Metabolite set enrichment analysis (MSEA) identifies potential disruption of
358 several diverse biochemical pathways including amino acid metabolism,
359 glycolysis/gluconeogenesis, nicotinate and nicotinamide metabolism, and purine metabolism
360 (**Figure 5B**).

361

362 **Retinal NMNAT1 loss causes disruption of NAD biosynthetic pathways and central carbon**
363 **metabolism**

364 As a first step in our metabolomics analysis, we characterized changes to retinal NAD^+
365 biosynthetic pathways upon NMNAT1 ablation (**Figure 5C,D**). At P4, knockouts show a ~40%
366 reduction of total retinal NAD^+ levels and levels of nicotinic acid adenine dinucleotide (NaAD),
367 the other catalytic product of NMNAT1 (**Figure 5C,D**). Levels of the downstream metabolites
368 NADP and nicotinamide (NAM) were decreased by ~25% and ~55%, respectively, while levels
369 of NADH were decreased but not significantly (**Figure 5C**). As expected, we observe significant
370 accumulation of NAD precursors nicotinamide riboside (NR) and nicotinamide mononucleotide

371 (NMN) in P4 knockout retinas (**Figure 5C**). Interestingly, we observe no significant changes in

372 levels of tryptophan, the starting point for de novo NAD synthesis, at this age (**Figure 5C,D**).

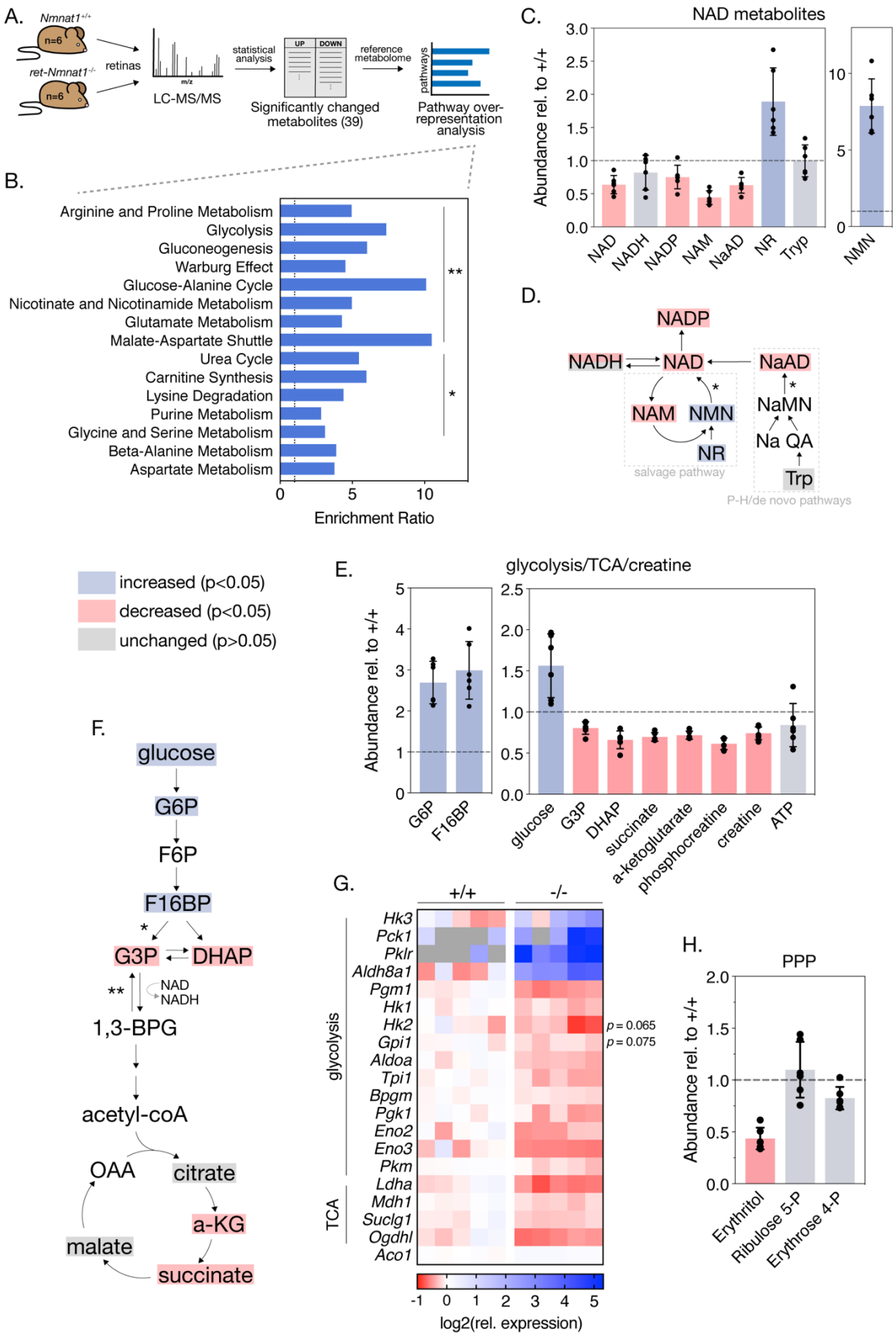
A.
Nmnat1+/+
n=6
ret-Nmnat1-/-
n=6
retinas
LC-MS/MS
statistical analysis
UP
DOWN
Significantly changed metabolites (39)
reference metabolome
pathways
Pathway over-representation analysis
B.
Arginine and Proline Metabolism
Glycolysis
Gluconeogenesis
Warburg Effect
Glucose-Alanine Cycle
Nicotinate and Nicotinamide Metabolism
Glutamate Metabolism
Malate-Aspartate Shuttle
Urea Cycle
Carnitine Synthesis
Lysine Degradation
Purine Metabolism
Glycine and Serine Metabolism
Beta-Alanine Metabolism
Aspartate Metabolism
**
*
0
5
10
Enrichment Ratio
C.
NAD metabolites
Abundance rel. to +/+
NAD
NADH
NADP
NAM
NaAD
NR
Tryp
NMN
D.
NADP
NADH
NAD
NaAD
NAM
NMN
NR
salvage pathway
NaMN
Na QA
Trp
P-H/de novo pathways
increased (p<0.05)
decreased (p<0.05)
unchanged (p>0.05)
E.
glycolysis/TCA/creatine
Abundance rel. to +/+
G6P
F16BP
glucose
G3P
DHAP
succinate
a-ketoglutarate
phosphocreatine
creatine
ATP
F.
glucose
G6P
F6P
F16BP
G3P
DHAP
NAD
NADH
1,3-BPG
acetyl-coA
OAA
citrate
a-KG
malate
succinate
G.
+/+
-/-
Hk3
Pck1
Pklr
Aldh8a1
Pgm1
Hk1
Hk2
Gpi1
Aldoa
Tpi1
Bpgm
Pgk1
Eno2
Eno3
Pkm
Ldha
Mdh1
Suclg1
Ogdhl
Aco1
glycolysis
TCA
p = 0.065
p = 0.075
log2(rel. expression)
H.
PPP
Abundance rel. to +/+
Erythritol
Ribulose 5-P
Erythrose 4-P

373

374 **Figure 5. Loss of NMNAT1 impairs retinal central carbon metabolism.** (**A**) schematic
375 illustrating metabolomics experimental approach. (**B**) results of metabolite set enrichment
376 analysis (MSEA) on significantly changed metabolites in P4 knockout retinas. (**C**) relative
377 abundance of NAD^+ pathway metabolites in P4 knockout retinas as assessed by mass
378 spectrometry. (**D**) schematic illustrating the major mammalian NAD^+ synthesis pathways colored
379 according to metabolite changes in (**C**); NMNAT1-catalyzed steps are indicated with asterisks.
380 (**E**) relative abundance of glycolysis, TCA cycle, and creatine metabolites in P4 knockout retinas
381 as assessed by mass spectrometry. (**F**) schematic depicting abbreviated glycolysis/TCA cycle
382 pathway colored according to metabolite changes in (**E**); aldolase-catalyzed step is indicated by a
383 single asterisk, while GAPDH-catalyzed step is marked with a double asterisk. (**G**) heatmap of
384 log-transformed relative expression of a set of glycolysis/TCA cycle genes in P4 knockout (-/-)
385 and control retinas (+/+) as assessed by RNA-sequencing. (**H**) relative abundance of pentose-
386 phosphate pathway (PPP) metabolites in P4 knockout retinas as assessed by mass spectrometry.
387 Data are represented as mean ± SD. n=6 biological replicates for (**B,C,E,H**), n=5 biological
388 replicates for (**G**).
389

390 Interestingly, the set of significantly changed metabolites in P4 knockout retinas is enriched for
391 metabolites associated with glycolysis, gluconeogenesis, and the Warburg effect (**Figure 5B**).
392 Closer examination of these pathways reveals large relative increases in levels of the upstream
393 glycolytic metabolites glucose, glucose 6-phosphate (G6P) and fructose 1,6-bisphosphate
394 (F16BP), as well as significant decreases in levels of dihydroxyacetone phosphate (DHAP) and
395 glucose 3-phosphate (G3P) (**Figure 5E, F**), strongly suggesting a disruption to forward
396 glycolytic flux. Consistent with such an effect, levels of the TCA cycle intermediates alpha-
397 ketoglutarate (a-KG) and succinate are decreased by ~30% in P4 knockout retinas (**Figure 5E,**
398 **F**). Further in line with disruptions to downstream mitochondrial metabolism, we observe
399 reduction of several acylcarnitine species at this age as well (**Figure 5—Supplement 1, panel**
400 **A**). Interestingly, although we observe decreased levels of the ATP-recycling metabolites
401 phosphocreatine and creatine at P4, retinal ATP levels at this age are slightly but not
402 significantly reduced ($p = 0.5$) (**Figure 5F**).
403
404 To further investigate possible glycolytic disruptions in P4 knockout retinas, we assayed the
405 expression of a collection of glycolysis and TCA cycle enzymes in P4 knockout and control
406 retinas using our RNA-sequencing dataset. Indeed, this analysis reveals broad transcriptional
407 changes in 16 glycolytic and 4 TCA cycle enzymes in P4 knockout retinas (**Figure 5G**).
408 Notably, two of these changes—upregulation of the aldehyde dehydrogenase *Aldh8a1* and
409 downregulation of the TCA cycle enzyme *Ogdhl*—are also present in RNA-sequencing results
410 from the pre-degenerative (E18.5) timepoint (**Figure 5—Supplement 1, panel B**). Finally,
411 consistent with disruption of glycolytic flux and reduced NADP levels in knockout retinas, mass

412 spectrometry suggests possible disruption of the pentose phosphate pathway (PPP) evidenced by
413 decreased levels of erythritol at this age (**Figure 5H**).
414
415 **NMNAT1 loss disrupts retinal purine metabolism and a subset of amino acids**
416 As MSEA also indicated possible disruptions of purine metabolism and several amino acid
417 pathways in P4 NMNAT1 knockout retinas (**Figure 5B**), we closely examined levels of a
418 collection of metabolites representing most major nucleotide and amino acid metabolites in P4
419 knockout and control retinas (**Figure 5—Supplement 2**). Interestingly, while levels of the
420 pyrimidine nucleotide derivatives uracil, UDP, and cytidine were unchanged at this age, levels of
421 the purine nucleotide precursor xanthine, guanine, and GMP were increased by ~150%, ~147%,
422 and ~58%, respectively (**Figure 5—Supplement 2, panel A**). The sole affected pyrimidine
423 nucleotide was cytosine, which showed an impressive ~352% increase in P4 knockout retinas as
424 compared to controls (**Figure 5—Supplement 2, panel A**). In addition to defects in purine
425 metabolism, we observe significant changes in a subset of 10 amino acids and amino acid
426 derivatives in P4 knockout retinas including acetyl-asparagine and acetyl-lysine (**Figure 5—**
427 **Supplement 2, panel B**).
428
429 Overall, these metabolomics results reveal that NMNAT1 is likely responsible for maintaining
430 ~40% of the total retinal NAD^+ pool. Furthermore, they suggest specific disruptions to central
431 carbon, purine nucleotide, and amino acid metabolism as potential causes for severe retinal
432 degeneration in the absence of NMNAT1.
433

434 **DISCUSSION**

435

436 **NMNAT1-deficiency is associated with early and severe retinal degeneration involving**

437 **multiple cell types**

438 In this study, we demonstrate that retinal NMNAT1 deficiency in mice leads to severe

439 degeneration of photoreceptor, bipolar, and amacrine neurons soon after birth. In general, this

440 phenotype is consistent with several recent studies reporting partial or complete ablation of

441 retinal NMNAT1. One such study deletes NMNAT1 pan-retinally during development using

442 *Chx10-Cre* and reports degeneration of the ONL and INL starting after P2 and largely complete

443 by P15 (Eblimit et al., 2018). In a recent study which reported global ablation of NMNAT1 in

444 mature mice using a tamoxifen-inducible actin-Cre, while it took ~23 days post-tamoxifen

445 administration for retinal degeneration to begin, this degeneration was largely complete 10 days

446 thereafter (Sasaki et al., 2020a). Finally, two models featuring NMNAT1 ablation in developing

447 photoreceptors using *Crx-Cre* have been reported, both of which show a similar albeit slower

448 degeneration of the ONL and INL beginning around P6 and nearly total by P28 (Wang, et al.,

449 2017; Eblimit et al., 2018). While the present study supports a relatively rapid timeline of

450 NMNAT1-associated retinal degeneration, it furthers the characterization of this phenotype in

451 two important ways: first, by assessing the survival of specific retinal neuron subpopulations,

452 and second, by systematically examining retinal cell death pathways triggered by NMNAT1

453 deletion.

454

455 Examination of specific cell type markers in NMNAT1 knockout retinas reveals that, while

456 photoreceptors are likely the primary targets of NMNAT1-associated pathology, retinal bipolar

457 and amacrine cells are also sequentially and significantly affected by loss of NMNAT1 during
458 retinal development, while ganglion cells appear unaffected until later stages. Interestingly, this
459 differential sensitivity is mirrored in our transcriptomics analyses, which demonstrate robust
460 deregulation of a cluster of photoreceptor and several bipolar cell-specific genes but relatively
461 few changes in amacrine or ganglion specific genes. These results stand partially in contrast to a
462 recent study reporting *ex vivo* knockdown of NMNAT1 in retinal explant cultures, which
463 reported thinner INLs but no changes in numbers of HuC/D-expressing amacrine cells or PKCa-
464 expressing bipolar cells in NMNAT1-deficient explants (Kuribayashi et al., 2018). However, this
465 study did report reduced numbers of PNR-positive photoreceptor cells in NMNAT1-deficient
466 explants, and we believe that differences regarding amacrine and bipolar cell effects can be
467 explained by the fact that NMNAT1 expression in explants was knocked down relatively late in
468 development (E17.5) as compared to the E9.5 activation of Six3-Cre (Furuta et al, 2000).
469
470 While we were unable to successfully determine retinal NMNAT1 distribution using our
471 polyclonal NMNAT1 antibody, previously published results showing RT-qPCR of *Nmnat1*,
472 *Nmnat2*, and *Nmnat3* levels in whole retinal lysate and flow-sorted $Cd73^+$ rod photoreceptors
473 suggest that NMNAT1 is the predominantly expressed NMNAT isoform in rod photoreceptors
474 (Kuribayashi et al., 2018). Combined with our data confirming a lack of transcriptional
475 upregulation of either *Nmnat2* or *Nmnat3* in NMNAT1 knockout retinas (**Figure 3—**
476 **Supplement 1**), one possible explanation for the cell-type specific degeneration we observe is
477 that relatively higher levels of NMNAT2 in inner retinal neurons can partially compensate for
478 the NAD^+ deficit caused by loss of NMNAT1. Overall, our results demonstrate that NMNAT1 is

479 crucial for the early survival of photoreceptors, bipolar cells, and amacrine cells, and facilitates
480 future work in identifying possible retinal cell-type specific requirements of NAD^+ metabolism.
481
482 **The severity of NMNAT1-associated retinal degeneration is associated with activation of**
483 **multiple cell death pathways**
484 Previous reports of cell death in NMNAT1-deficient retinas center on two potentially contrasting
485 mechanisms: the aforementioned *ex vivo* study outlined a role for *Noxa* and *Fas*-associated,
486 caspase-3 dependent apoptosis in NMNAT1-deficient explants (Kuribayashi et al., 2018), while
487 a more recent study found the death of mature photoreceptors after global NMNAT1 deletion to
488 be exquisitely dependent on the neuronal NADase SARM1 (Sasaki et al., 2020a). Using both
489 histological and comprehensive transcriptomic approaches, we demonstrate involvement of
490 caspase-3 associated apoptosis in NMNAT1 knockout retinas characterized by an early and
491 sustained upregulation of *Noxa* and deregulation of several other apoptosis-pathway genes. We
492 extend these results by showing histological evidence of a distinct, caspase-3 independent cell
493 death pathway which constitutes a significant portion of observed cell death and closely follows
494 caspase-3 dependent apoptosis throughout the timepoints tested in our model. Interestingly,
495 utilizing a recently validated and highly-touted metabolic marker of SARM1 activity (Sasaki et
496 al., 2020b), as well as assessing baseline *Sarm1* levels, we do not find evidence of SARM1
497 involvement at either pre- or post-degenerative timepoints in our model. Instead, our
498 transcriptomics results indicate deregulation of several pyroptosis and necroptosis-related genes,
499 notably including the entire "canonical inflammasome" (*Casp1*, *Nlrp3*, and *Pycard*), as well as
500 the toll-like receptors *Tlr2* and *Tlr4*, at pre- and post-degenerative timepoints (**Figure 4**).
501

502 Although cell death pathways are largely interconnected and notoriously complex (Vandenabeele
503 et al., 2010; Newton et al., 2014; Preyat and Leo 2015; Muller et al., 2017; Swanson et al.,
504 2019;), several lines of evidence support the potential involvement of pyroptosis in our model
505 over alternative pathways. Included among these is the distinct presence of nuclear pyknosis
506 (chromatin condensation) in caspase-3 negative dying cells, which is generally incompatible with
507 necroptosis but has been observed in pyroptotic cells (Vandenabeele et al., 2010; Murakami et
508 al., 2012; Miao et al., 2011). In addition to observing upregulation of a collection of pyroptosis-
509 associated genes, a relatively large upregulation of *Nlrp3* in E18.5 NMNAT1 knockout retinas is
510 consistent with a well-characterized transcriptional "priming" step of pyroptosis (Swanson et al.,
511 2019). Curiously, while we do not detect proteolytic cleavage of gasdermin D—a common
512 marker of pyroptosis—in P4 NMNAT1 knockout retinas (**Figure 4—Supplement 1**), we do
513 observe transcriptional upregulation of the related gasdermin C4 (*Gsdmc4*), for which no
514 commercial antibody is currently available. Furthermore, recent results indicate that NLRP3 is,
515 under certain circumstances, capable of being activated independently of gasdermin D (Gutierrez
516 et al., 2017). With regard to several changes to ferroptosis-associated genes, their relatively small
517 number and presence only at post-degenerative timepoints argues for involvement as secondary
518 to other cell death pathways. Finally, considering a very recent report suggesting involvement of
519 the PARP1-associated 'parthanatos' cell death pathway in NMNAT1 mutant retinas (Greenwald
520 et al., 2021), we did not detect accumulation of poly ADP-ribose (PAR) in caspase-3 negative
521 pyknotic nuclei (data not shown), arguing against involvement of this pathway under these
522 conditions.
523

524 That we do not find evidence of SARM1 involvement, even in the presence of increased levels
525 of its potent activator NMN (Zhao et al., 2019; Figley et al., 2021) is unexpected but not
526 implausible, especially considering the fact that the report implicating SARM1 in NMNAT1-
527 associated degeneration deleted NMNAT1 in mature mice (Sasaki et al., 2020a). Indeed, the
528 phenomenon of age-dependent susceptibility of the retina to different cell death pathways is
529 well-documented—in particular, many apoptosis effectors (*Casp3*, *Casp9*, *Apaf1*, *Bcl* family
530 members) active in the developing mammalian retina are subsequently downregulated in mature
531 retinas, necessitating alternative death pathways for handling pathological insults at these ages
532 (Donovan and Cotter 2002; Doonan et al., 2003; Donovan et al., 2006). Considering these
533 results, it is wholly possible that in mature retinas with insufficient expression of necessary
534 apoptotic and/or pyroptotic machinery, NMNAT1-associated retinal degeneration proceeds
535 through SARM1—in such a case, it is important to note that model systems with embryonic or
536 germline deletion or mutation of NMNAT1 are typically more representative of patients with
537 disease-linked mutations in NMNAT1. On the other hand, it cannot be conclusively ruled out
538 that excess cADPR produced by an active SARM1 in our model is rapidly metabolized, and
539 recently described links between SARM1 and both pyroptosis and apoptosis (Mukherjee et al.,
540 2015; Carty et al., 2019) leave open the possibility of cooperation between these cell death
541 pathways in NMNAT1 knockout retinas.
542
543 Despite leaving open questions regarding the specific pathways involved in retinal degeneration
544 following embryonic NMNAT1 deletion, our results support and extend previously reported *ex*
545 *vivo* findings of a central role for *Noxa*- and *Fas*- associated apoptosis in NMNAT1-deficient
546 retinas and contest the SARM1-dependent photoreceptor death described in mature NMNAT1-

547 deficient retinas. A more comprehensive, transcriptomics-guided approach in the present study
548 reveals previously unknown complexity in NMNAT1-associated retinal degeneration; in
549 particular, activation of multiple distinct cell death pathways following NMNAT1 deletion may
550 explain the severity of the resulting phenotype. Future work will focus on definitively addressing
551 potential SARM1 involvement as well as systematically interrogating non-apoptotic cell death
552 pathways to gain a more complete phenotypic understanding of the NMNAT1-deficient retina.
553
554 Finally, we note that although the model presented here differs in important ways from
555 NMNAT1-mutant LCA animal models, it does recapitulate some aspects of NMNAT1-linked
556 LCA including particularly severe central retinal defects (Kumaran et al., 2017). As recent
557 studies have discovered noncoding mutations, copy number variations, and exon duplications in
558 NMNAT1 causing severe downregulation of NMNAT1 in patients with ocular and extra-ocular
559 pathologies (Coppieters et al., 2015; Bedoni et al., 2020), understanding the mechanisms of
560 retinal dysfunction in an NMNAT1 knockout model is of clinical significance.
561
562 **Metabolic defects in NMNAT1 knockout retinas**
563
564 While several recent studies examine levels of isolated metabolites in mature NMNAT1-
565 deficient retinas (Sasaki et al., 2020a), or more broadly examine tissue metabolomes after
566 perturbation of the NMN-synthesizing enzyme NAMPT (Lin et al., 2016; Oakey et al., 2019;
567 Lundt et al., 2021), the present study is—to our knowledge—the first to comprehensively define
568 global metabolic defects in any tissue after deletion of NMNAT1. Our metabolomics results
569 approximate that NMNAT1 is responsible for synthesizing ~40% of the total retinal NAD^+ pool,

570 a figure which is generally consistent with a previous model (Sasaki et al., 2020a). In addition,
571 our results strongly suggest that—via specific disruptions to central carbon, nucleotide, and
572 amino acid metabolism—depletion of NAD^+ synthesized in the nucleus by NMNAT1 has
573 distinct extra-nuclear effects in the retina. This is consistent with studies describing some level of
574 coordination between cytosolic, mitochondrial, and nuclear NAD^+ pools in non-retinal tissues
575 (Cambronne et al., 2016); however, whether these observations reflect a direct export of nuclear
576 NAD^+ to cytosolic and mitochondrial retinal compartments versus an indirect effect on cytosolic
577 and mitochondrial cellular processes (by way of NAD^+-dependent gene regulation, for instance)
578 is a topic for further study.
579
580 The existence of the aforementioned metabolomics studies on tissues deficient in NAMPT,
581 which catalyzes the NAD^+ synthesis step immediately prior to the NMNAT1-catalyzed step and
582 exhibits dynamic subcellular localization (Svoboda et al., 2019), permits identification of
583 potential NMNAT1-specific metabolic changes. Impaired glycolytic flux appears to be a more
584 general feature of tissue NAD^+ depletion, as studies reporting NAMPT inhibition or deletion in
585 projection neurons and skeletal muscle myotubes report accumulation of glycolytic metabolites
586 upstream of GAPDH (Oakey et al., 2019; Lundt et al., 2021). Furthermore, utilizing stable
587 isotope tracers, Lundt et al. present evidence that glycolysis blockage reverses glycolytic flux in
588 NAMPT-inhibited myotubes, an effect which we believe may explain decreased levels of G3P
589 and DHAP in our model. Notably, unbiased LC-MS/MS and GC-MS analyses of rod-
590 photoreceptor-specific NAMPT knockout retinas showed signatures of mitochondrial metabolic
591 defects—which we observe in our model as well—but detected limited evidence of glycolytic
592 impairment (Lin et al., 2016). This raises the possibility that retinal NMNAT1 and NAMPT

593 depletion, despite both lowering total retinal NAD^+ levels, produce distinct metabolic
594 phenotypes.
595
596 Retinal neurons—and retinal photoreceptors in particular—are relatively unique in their
597 dependence on aerobic glycolysis (the "Warburg Effect") during both proliferative and
598 differentiated states (Agathocleous et al., 2012; Ng et al., 2015; Chinchore et al., 2017). Our
599 finding that retinal NMNAT1 loss is detrimental to glycolysis thus offers a potential explanation
600 for the cell type-specific degeneration which we observe: in particular, results indicating that
601 differentiation induces an increased reliance on mitochondrial OXPHOS relative to glycolysis in
602 the retina might explain why ganglion and amacrine cells, which differentiate relatively early in
603 retinogenesis, are less sensitive to NMNAT1 loss in our model than the later born bipolar and
604 photoreceptor cells (Agathocleous et al., 2012). Indeed, even in mature retinas, perturbations to
605 glycolysis robustly and specifically affect photoreceptor health and survival (Chinchore et al.,
606 2015; Zhang et al., 2020; Sinha et al., 2021). Interestingly, we find no significant change in
607 retinal ATP levels at P4, arguing against the parsimonious assumption of bioenergetic collapse as
608 the cause of the severe cell death which we observe. Furthermore, recent results implicating
609 glycolytic flux impairment in NLRP3 activation provide a potential link between metabolic
610 defects and non-apoptotic cell death which we observe in NMNAT1 knockout retinas (Sanman
611 et al., 2016).
612
613 In addition to glycolytic impairment, we note specific defects in purine nucleotide and amino
614 acid metabolic pathways in NMNAT1 knockout retinas. As a particularly proliferative tissue—
615 owing primarily to photoreceptors' continuous renewal of their light-sensing 'outer segment'

organelles—the retina is thought to be particularly reliant on adequate nucleotide and amino acid pools to support transcription and translation of outer segment machinery (Etingof 2001; Ng et al., 2015). Some of the metabolic changes which we observe—for instance, accumulation of the purine precursor xanthine and the amino acid aspartate—appear to be more widely associated with NAD^+ insufficiency or retinal degeneration (Du et al., 2014; Lin et al., 2016; Oakey et al., 2019). On the other hand, we also identify a collection of metabolic changes in these pathways which are not reported in NAMPT-deficient retinas (Lin et al., 2016), potentially explaining differences in retinal phenotypes between these two models. Further investigation in this direction should include metabolite flux analyses and spatial metabolomics methods to clarify the mechanisms involved.

A potential role for NMNAT1 in photoreceptor terminal differentiation

The tightly coordinated and stereotypical differentiation of retinal neuron subtypes from a common progenitor pool has been extensively studied—complementing classical birth-dating studies, recent high-profile investigations have begun to explore the massive epigenetic regulation necessary for the development of the mammalian retina (Swaroop et al., 2010; Raeisossadati et al., 2021). One of the most surprising findings of the present study is an early and sustained transcriptional downregulation of a relatively small set of photoreceptor- and synapse-specific genes in NMNAT1 knockout retinas. Beyond these transcriptional disruptions, we show near complete absence of rhodopsin and recoverin protein in P4 NMNAT1 knockout retinas. While NMNAT1 has previously been implicated in gene regulation through direct interaction with SIRT1 and PARP1 at gene promoters (Zhang et al., 2012; Song et al., 2013) and

639 NMNAT1 knockdown was shown to influence apoptotic gene expression by potentially
640 modulating histone acetylation (Kuribayashi et al., 2018), no *in vivo* role for NMNAT1 in retinal
641 developmental gene regulation has yet been described.
642
643 Photoreceptors are among the last retinal cell types to fully develop, and their developmental
644 programs can be split into two broad phases: an early phase comprising commitment to the
645 photoreceptor cell fate, mediated by several well-characterized transcription factors including
646 OTX2, NRL, and CRX, and a later phase comprising expression of a host of specialized
647 phototransduction genes and outer segment biogenesis ("terminal differentiation") (Swaroop et
648 al., 2010; Brzezinski and Reh, 2015; Daum et al., 2017). Interestingly, we do not observe
649 transcriptional changes in OTX2, NRL, CRX, or related genes in NMNAT1 knockout retinas at
650 either tested age. This fact, combined with grossly normal retinal morphology at P0, suggests
651 that NMNAT1 is required for terminal differentiation but not early specification or proliferation
652 of both rod and cone photoreceptor cells. Increased abundance of acetyl-lysine in knockout
653 retinas on mass spectrometry (**Figure 6B**) and GO enrichment of several genes associated with
654 DNA methylation, epigenetic regulation, and chromatin silencing in P4 knockout retinas (**Figure**
655 **3—Supplement 2**) support a potential role for NMNAT1 in the epigenetic regulation of
656 photoreceptor terminal differentiation, a phenomenon recently shown to feature genome-wide
657 methylation and acetylation events (Aldiri et al., 2017).
658
659 Many potential routes exist between NMNAT1-catalyzed nuclear NAD^+ synthesis and retinal
660 gene regulation—these include histone- and gene-level regulation by NAD^+-dependent SIRTs
661 and PARPs as well as NAD^+-dependent DNA methylation or alpha-ketoglutarate dependent

662 hydroxymethylation mediated by DNA-methyltransferase (DNMT) or TET family enzymes,
663 respectively (Chang et al., 2010; Seritrakul and Gross, 2017). While the precise mechanisms of
664 NMNAT1-associated retinal gene dysregulation are currently under investigation, we note that
665 many of the photoreceptor genes downregulated in our study are dynamically demethylated
666 during retinal development (Dvoriantchikova et al., 2019), and that perturbation of the DNA
667 methyltransferases DNMT1, DNMT3A, and DNMT3B in the retina produces similar phenotypes
668 to those observed in the current study (Rhee et al., 2012; Singh et al., 2017).
669
670 In conclusion, this study presents the most comprehensive evaluation of NMNAT1-associated
671 retinal dysfunction to date and suggests crucial roles for nuclear NAD^+ in the proper
672 development and early survival of the mammalian retina. While we provide evidence that the
673 early and severe retinal degeneration associated with NMNAT1 loss involves multiple cell types
674 and death pathways, it appears that this severe phenotype stems from two major problems: 1.)
675 metabolic defects likely caused by insufficient NAD^+ for retinal proliferative metabolism, and 2.)
676 gene regulation defects potentially caused by insufficient nuclear NAD^+ in developing
677 photoreceptors. Considering intriguing links between metabolic state and differentiation in the
678 retina and recently discovered roles of compartmentalized NAD^+ in non-retinal cell
679 differentiation (Agathocleous et al., 2012; Agathocleuous et al., 2013; Ryu et al., 2018), these
680 two problems may not be mutually exclusive. Further study of NMNAT1-associated retinal
681 dysfunction should focus on evaluating the relative contributions of metabolic and genetic
682 deficits to the overall pathology and testing the hypothesis that NMNAT1 functions to integrate
683 retinal energy metabolism and gene regulation.
684

685

686 **MATERIALS AND METHODS**

687

688 **Animal Model Generation, Husbandry, and Genotyping**

689 *Nmnat1*$^{fl/fl}$ mice were described previously (Conforti 2011) were thoroughly backcrossed with
690 wild-type 129/SV-E mice (Charles River Laboratories, Wilmington, MA) prior to analyses.
691 Conditional knockout mice were generated by crossing *Nmnat1*$^{fl/fl}$ mice with transgenic mice
692 expressing Cre recombinase under a *Six3* promoter (*Six3-Cre*) (Christiansen et al., 2011).
693 Crosses yielded heterozygous *Nmnat*$^{fl/wt}$ and *Six3-Cre Nmnat*$^{fl/wt}$ offspring, which were further
694 crossed with *Nmnat1*$^{fl/fl}$ mice to yield conditional knockout (*Six3-Cre Nmnat*$^{fl/fl}$) and littermate
695 control (*Nmnat1*$^{fl/fl}$) mice at approximately Mendelian ratios. Experimental animals were
696 periodically backcrossed with wild-type 129/SV-E mice to maintain genetic integrity. Animals
697 were maintained under standard 12 hour light/dark cycles with food and water provided *ad*
698 *libitum*. All experimental procedures involving animals were approved by the Institutional
699 Animal Care and Use Committee (IACUC) of West Virginia University.

700

701 Animals were genotyped using polymerase chain reaction (PCR) of genomic DNA from ear
702 punch biopsies. Primer sequences for detection of *Six3-Cre* transgene and *Nmnat1* 5' and 3' loxP
703 sites are listed in **Supplementary Table 1**, and primers were added to the PCR reaction at a final
704 concentration of 0.75 μM. The thermocycling conditions were 95ºC for 2 minutes, 35 cycles of
705 95ºC for 30s, 58ºC for 30s, 72ºC for 45s, and a final extension step of 72ºC for 5 minutes.

706

707 **NMNAT1 Antibody Generation**

708 A rabbit polyclonal antibody against amino acids 111-133 of mouse NMNAT1 (sequence
709 CSYPQSSPALEKPGRKRKWADQK) was generated by Pacific Immunology Corp. (Pacific
710 Immunology, Ramona, CA). The affinity-purified antibody was confirmed to recognize
711 NMNAT1 in cell culture and retinal lysate (**Figure 1—Supplement 1**), and did not recognize
712 overexpressed FLAG-NMNAT2 (data not shown).
713
714 **Mammalian Cell Culture and Transfection**
715 HEK293T cells were maintained in 1:1 DMEM/F-12 culture media (Thermo Fisher Scientific,
716 Waltham, MA) in a sterile incubator at 37ºC and 5% CO_2. Transient transfection of FLAG-
717 NMNAT1 and FLAG-NMNAT2 constructs (see Supplemental Table 2) was performed at ~60%
718 confluence using TransIT®-LT1 transfection reagent (Mirus Bio, Madison, WI) according to
719 manufacturer's instructions. Cells were harvested 48 hours after transfection on ice with 1X
720 Hank's balanced salt solution (HBSS) (Thermo Fisher Scientific) and cell pellets were processed
721 for western blotting as described below.
722
723 **Retinal Histology and Thickness Quantification**
724 To evaluate gross retinal histology, mice at the indicated ages were sacrificed and their eyes were
725 gently removed into 1ml Excalibur's Alcoholic z-fix (Excalibur Pathology Inc., Norman, OK).
726 Subsequent fixation, paraffin embedding, sectioning, and hematoxylin and eosin (H&E) staining
727 were performed by Excalibur Pathology. H&E-stained sections were imaged on a Nikon Eclipse
728 Ti microscope with DS-Ri2 camera (Nikon Instruments, Melville, NY). Retinal thickness was
729 measured using Nikon NIS-Elements software at 4 equidistant points along the outer retinal edge
730 to either side of the optic nerve, where retinal thickness is defined as the length of a line

731 orthogonal to the outer retinal edge and terminating at the inner retinal edge. Thickness was
732 quantified using 6 technical replicates per animal and 3 biological replicates per genotype.
733
734 **Western Blotting**
735 For determination of protein levels by western blot, retinas were homogenized in cold lysis
736 buffer (1X phosphate-buffered saline pH 7.4 (Thermo Fisher Scientific), Pierce® protease
737 inhibitor, EDTA-free (Thermo), Calbiochem® phosphatase inhibitor cocktail (EMD Biosciences,
738 La Jolla, CA)) using a Microson® ultrasonic cell disruptor. Protein concentration was determined
739 using a Nanodrop ND-1000 spectrophotometer (Thermo Fisher Scientific), after which Laemmli
740 sample buffer was added to a final concentration of 1X (2% SDS, 0.05M Tris-HCl pH 6.8, 10%
741 glycerol, 1% β-mercaptoethanol, 2 mM dithiothreitol (DTT), 0.001% bromphenol blue) and
742 samples were boiled for 5 minutes. Equal amounts of protein were separated on anykD® mini-
743 PROTEAN TGX polyacrylamide gels (Bio-Rad, Hercules, CA) and transferred to an
744 Immobilon-FL PVDF membrane (Millipore, Burlington, MA). Membranes were blocked with
745 Odyssey® blocking buffer (LI-COR Biosciences, Lincoln, NE) for 1 hour at room temperature
746 and incubated with primary antibodies diluted in 50/50 blocking buffer/1X PBST (1X PBS +
747 0.1% Tween-20) at 4ºC overnight on a bidirectional rotator. A list of primary antibodies, sources,
748 and dilutions can be found in **Supplemental Table 2**. Following primary antibody incubations,
749 membranes were washed in 1X PBST and incubated with goat anti-rabbit Alexa Fluor 680
750 and/or goat anti-mouse DyLight 800 secondary antibodies (Thermo Fisher Scientific) for 1 hour
751 at room temperature. Membranes were subsequently washed in 1X PBST and imaged using an
752 Odyssey Infrared Imaging System (LI-COR Biosciences).
753

754 **Quantitative Reverse Transcriptase-PCR (RT-qPCR)**

755 To determine relative gene expression using RT-qPCR, retinas were collected and total RNA
756 was isolated as described below. cDNA was synthesized with a RevertAid® cDNA Synthesis Kit
757 (Thermo Fisher Scientific) per manufacturer instructions, starting with 1μg total RNA/sample
758 and using random hexamer primers. Primers for targets of interest were designed using NCBI
759 Primer-BLAST (https://www.ncbi.nlm.nih.gov/tools/primer-blast/) to straddle at least one intron
760 of length >500bp. qPCR reactions were performed using Brilliant II SYBR® Green qPCR
761 master mix with low ROX (Agilent Technologies, Cedar Creek, TX) and monitored on a
762 Stratagene® Mx3000P cycler (Agilent Technologies). Prior to use, primers were validated (by
763 examining melt curves and agarose gel electrophoresis) to amplify single products of expected
764 size. Three technical replicates per target per animal were performed, and averages from three
765 animals per genotype are reported. All expression values were normalized to the geometric
766 average of three housekeeping genes (*Hmbs*, *Ppia*, and *Ywhaz*).

767

768 **Immunofluorescent Staining**

769 After euthanasia, eyes were gently removed, punctured, and immersed in 4% paraformaldehyde
770 fixative (4% paraformaldehyde in 1X PBS) (Electron Microscopy Sciences, Hatfield, PA) for 15
771 minutes, after which the cornea was removed and the eye was fixed for an additional 45 minutes
772 at room temperature with gentle agitation. Subsequently, eyes were washed in 1X PBS and
773 incubated in a dehydration solution (20% sucrose in 1X PBS) for at least 12 hours at 4ºC. After
774 dehydration, samples were incubated in a 1:1 mixture of 20% sucrose and Tissue-Tek® O.C.T.
775 compound (Sakura Finetek, Torrance, CA) for at least 1 hour before being transferred to 100%
776 O.C.T. and flash frozen. 16 μm sections were cut using a Leica CM1850 cryostat (Leica

777 Biosystems, Nussloch, Germany) and mounted on Superfrost Plus slides (Fisher Scientific). For
778 immunofluorescent staining, retinal sections were briefly rinsed with 1X PBS and incubated in
779 blocking buffer (10% normal goat serum, 0.5% Triton X-100, 0.05% sodium azide in 1X PBS)
780 for 1 hour at room temperature. Following blocking, sections were incubated with the indicated
781 primary antibodies (diluted in buffer containing 5% normal goat serum, 0.5% Triton X-100,
782 0.05% sodium azide in 1X PBS) overnight at 4ºC. The next day, sections were washed with 1X
783 PBST and incubated with DAPI nuclear stain (Thermo Fisher Scientific), goat anti-rabbit Alexa
784 Fluor-568 and/or goat anti-mouse Alexa Fluor-488 (Thermo Fisher Scientific) secondary
785 antibodies for 1 hour at room temperature. For antibody information and dilutions, see
786 **Supplemental Table 2**. Finally, sections were washed, cover-slipped with Prolong Gold®
787 antifade reagent (Thermo Fisher Scientific), and imaged on a Nikon Eclipse Ti laser scanning
788 confocal microscope with C2 camera (Nikon Instruments). Experimental and control sections
789 were imaged using identical laser intensity and exposure settings. All fluorescent images
790 represent maximum intensity z-projections generated using ImageJ with the Bio-Formats plugin
791 (https://imagej.net/Bio-Formats).
792
793 **Retinal Cell Type and Caspase-Positive Cell Quantification**
794 To estimate numbers of pyknotic and caspase-3 positive/negative cells in retinas of knockout and
795 control mice, pyknotic nuclei were manually counted in 212.27 x 212.27 μm^2 regions of
796 maximum intensity projection fluorescent images from the central retina. Once these pyknotic
797 nuclei were identified, the number also labeled with active-Caspase-3 were manually counted.
798 Counts from two technical replicates per animal were averaged, and averages from three animals
799 per genotype are reported. Counts of retinal cell subtypes were estimated by manually counting

800 marker-positive cells in 318.2 x 318.2 μm^2 regions of central retina, averaged between two
801 technical replicates per animal and three animals per genotype. All counts were obtained using
802 ImageJ. For antibody information, see **Supplemental Table 2**.
803
804 **Retinal RNA Extraction, Sequencing, and Analysis**
805 Following euthanasia and eye enucleation, retinae were quickly dissected and transferred into
806 ultra-sterile microcentrifuge tubes containing a small amount of Trizol® reagent (Thermo Fisher
807 Scientific), and flash frozen on dry ice. Total RNA was extracted by homogenizing thawed
808 samples with a handheld homogenizer and incubating for 5 min. at room temperature. 20μl
809 chloroform was added to each sample, samples were briefly vortexed, incubated at room
810 temperature for 4 min., and spun at 12,000 rpm for 10 min. at 4ºC. The aqueous layers were
811 removed to separate tubes containing 50μl isopropanol and incubated at room temperature for 10
812 min. with occasional agitation. Finally, samples were again spun at 12,000 rpm for 10 min. at
813 4ºC, supernatants were removed, and pellets were washed three times with 75% ethanol, dried,
814 and resuspended in DEPC-treated water. Whole-transcriptome sequencing was performed by
815 Macrogen Corp. (Macrogen USA, Rockville, MD) using an Illumina TruSeq Stranded mRNA
816 Library Prep Kit on a NovaSeq6000 S4 to a depth of 100M total reads per sample. Read quality
817 was verified using FastQC (https://www.bioinformatics.babraham.ac.uk/projects/fastqc/) and
818 adapters were trimmed using the Bbduk utility of the BBTools package
819 (http://sourceforge.net/projects/bbmap/). Read alignment was performed using HISAT2 2.1.0
820 (Kim et al., 2015) and transcripts were assembled and quantified using StringTie 1.3.6 (Pertea et
821 al., 2015; Pertea et al., 2016). Differentially expressed genes were identified using the DESeq2 R
822 package (Love et al., 2014).

823

824 **Targeted Steady-State Metabolomics using LC-MS/MS**

825 Following euthanasia and eye enucleation, retinae were quickly dissected into Hank's Balanced
826 Salt Solution (HBSS) and flash frozen on dry ice. Metabolites were extracted according to
827 previously described protocols (Du et al., 2015; Zhu et al., 2018). Metabolite extracts were
828 analyzed by a Shimadzu LC Nexera X2 UHPLC coupled with a QTRAP 5500 LC-MS/MS (AB
829 Sciex). An ACQUITY UPLC BEH Amide analytic column (2.1x50 mm, 1.7 µm) (Waters Corp.,
830 Milford, MA) was used for chromatographic separation. The mobile phase was (A) water with
831 10 mM ammonium acetate (pH 8.9) and (B) acetonitrile/water (95/5) with 10 mM ammonium
832 acetate (pH 8.2) (All solvents were LC–MS Optima grade from Fisher Scientific). The total run
833 time was 11 min. with a flow rate of 0.5 ml/min. and an injection volume of 5 µl. The gradient
834 elution was 95–61% B in 6 min, 61–44% B at 8 min, 61–27% B at 8.2 min, and 27–95% B at 9
835 min. The column was equilibrated with 95% B at the end of each run. The source and collision
836 gas was N_2. The ion source conditions in positive and negative mode were: curtain gas (CUR) =
837 25 psi, collision gas (CAD) = high, ion spray voltage (IS) = 3800/-3800 volts, temperature
838 (TEM) = 500 °C, ion source gas 1 (GS1) = 50 psi, and ion source gas 2 (GS2) = 40 psi. Each
839 metabolite was tuned with standards for optimal transitions. D4-nicotinamide (Cambridge
840 Isotope Laboratories, Tewksbury, MA) was used as an internal standard. The extracted MRM
841 peaks were integrated using MultiQuant 3.0.3 software (AB Sciex, Concord, ON, CA).

842

843 **Statistical Analyses**

844 Sample number (n) is defined as number of animals per genotype. Specific statistical tests and
845 sample sizes are indicated in figure legends. Where applicable, p-value adjustments for multiple

comparisons were performed and indicated, and reported as 'q' values. Across all figures, statistical significance is defined as $p<0.05$ (or $q<0.05$, where applicable). Experimenters were not blinded to treatments.

ACKNOWLEDGEMENTS

We thank Drs. Maxim Sokolov, Visvanathan Ramamurthy, and Peter Mathers for helpful comments and critical evaluation of the manuscript, and we thank current and past members of the Kolandaivelu lab for constant support. This work was supported by the National Eye Institute [RO1EY028959] and WVU startup funds to SK.

COMPETING INTERESTS

The authors declare no competing interests.

REFERENCES

Agathocleous, Michalis, and William A. Harris. "Metabolism in Physiological Cell Proliferation and Differentiation." Trends in Cell Biology 23, no. 10 (October 2013): 484–92. https://doi.org/10.1016/j.tcb.2013.05.004.

Aldiri, Issam, Beisi Xu, Lu Wang, Xiang Chen, Daniel Hiler, Lyra Griffiths, Marc Valentine, et al. "The Dynamic Epigenetic Landscape of the Retina During Development, Reprogramming, and Tumorigenesis." Neuron 94, no. 3 (May 2017): 550-568.e10. https://doi.org/10.1016/j.neuron.2017.04.022.

Aleman, Tomas S., Katherine E. Uyhazi, Leona W. Serrano, Vidyullatha Vasireddy, Scott J. Bowman, Michael J. Ammar, Denise J. Pearson, Albert M. Maguire, and Jean Bennett. "RDH12 Mutations Cause a Severe Retinal Degeneration With Relatively Spared Rod Function." Investigative Opthalmology & Visual Science 59, no. 12 (October 1, 2018): 5225. https://doi.org/10.1167/iovs.18-24708.

Bennett, Lea D., Martin Klein, Finny T. John, Bojana Radojevic, Kaylie Jones, and David G. Birch. "Disease Progression in Patients with Autosomal Dominant Retinitis Pigmentosa Due to a

Mutation in Inosine Monophosphate Dehydrogenase 1 (IMPDH1).” Translational Vision Science & Technology 9, no. 5 (April 23, 2020): 14. https://doi.org/10.1167/tvst.9.5.14.

Bowne, Sara J., Lori S. Sullivan, Sarah E. Mortimer, Lizbeth Hedstrom, Jingya Zhu, Catherine J. Spellicy, Anisa I. Gire, et al. “Spectrum and Frequency of Mutations in IMPDH1 Associated with Autosomal Dominant Retinitis Pigmentosa and Leber Congenital Amaurosis.” Investigative Opthalmology & Visual Science 47, no. 1 (January 1, 2006): 34. https://doi.org/10.1167/iovs.05-0868.

Brazill, Jennifer M, Chong Li, Yi Zhu, and R Grace Zhai. “NMNAT: It’s an NAD + Synthase… It’s a Chaperone… It’s a Neuroprotector.” Current Opinion in Genetics & Development 44 (June 2017): 156–62. https://doi.org/10.1016/j.gde.2017.03.014.

Brzezinski, Joseph A, and Thomas A Reh. “Photoreceptor Cell Fate Specification in Vertebrates,” 2015, 11.

Cambronne, X. A., M. L. Stewart, D. Kim, A. M. Jones-Brunette, R. K. Morgan, D. L. Farrens, M. S. Cohen, and R. H. Goodman. “Biosensor Reveals Multiple Sources for Mitochondrial NAD+.” Science 352, no. 6292 (June 17, 2016): 1474–77. https://doi.org/10.1126/science.aad5168.

Cambronne, Xiaolu A., and W. Lee Kraus. “Location, Location, Location: Compartmentalization of NAD+ Synthesis and Functions in Mammalian Cells.” Trends in Biochemical Sciences 45, no. 10 (October 2020): 858–73. https://doi.org/10.1016/j.tibs.2020.05.010.

Cantó, Carles, Keir J. Menzies, and Johan Auwerx. “NAD+ Metabolism and the Control of Energy Homeostasis: A Balancing Act between Mitochondria and the Nucleus.” Cell Metabolism 22, no. 1 (July 2015): 31–53. https://doi.org/10.1016/j.cmet.2015.05.023.

Carty, Michael, Jay Kearney, Katharine A. Shanahan, Emily Hams, Ryoichi Sugisawa, Dympna Connolly, Ciara G. Doran, et al. “Cell Survival and Cytokine Release after Inflammasome Activation Is Regulated by the Toll-IL-1R Protein SARM.” Immunity 50, no. 6 (June 2019): 1412-1424.e6. https://doi.org/10.1016/j.immuni.2019.04.005.

Chang, J., B. Zhang, H. Heath, N. Galjart, X. Wang, and J. Milbrandt. “Nicotinamide Adenine Dinucleotide (NAD)-Regulated DNA Methylation Alters CCCTC-Binding Factor (CTCF)/Cohesin Binding and Transcription at the BDNF Locus.” Proceedings of the National Academy of Sciences 107, no. 50 (December 14, 2010): 21836–41. https://doi.org/10.1073/pnas.1002130107.

Chiang, Pei-Wen, Juan Wang, Yang Chen, Quan Fu, Jing Zhong, Yanhua Chen, Xin Yi, et al. “Exome Sequencing Identifies NMNAT1 Mutations as a Cause of Leber Congenital Amaurosis.” Nature Genetics 44, no. 9 (September 2012): 972–74. https://doi.org/10.1038/ng.2370.

Chinchore, Yashodhan, Tedi Begaj, David Wu, Eugene Drokhlyansky, and Constance L Cepko. “Glycolytic Reliance Promotes Anabolism in Photoreceptors.” ELife 6 (June 9, 2017): e25946. https://doi.org/10.7554/eLife.25946.

Christiansen, J. R., S. Kolandaivelu, M. O. Bergo, and V. Ramamurthy. "RAS-Converting Enzyme 1-Mediated Endoproteolysis Is Required for Trafficking of Rod Phosphodiesterase 6 to Photoreceptor Outer Segments." Proceedings of the National Academy of Sciences 108, no. 21 (May 24, 2011): 8862–66. https://doi.org/10.1073/pnas.1103627108.

Conforti, Laura, Lucie Janeckova, Diana Wagner, Francesca Mazzola, Lucia Cialabrini, Michele Di Stefano, Giuseppe Orsomando, et al. "Reducing Expression of NAD+ Synthesizing Enzyme NMNAT1 Does Not Affect the Rate of Wallerian Degeneration." The FEBS Journal 278, no. 15 (2011): 2666–79. https://doi.org/10.1111/j.1742-4658.2011.08193.x.

Coppieters, Frauke, Anne Laure Todeschini, Takuro Fujimaki, Annelot Baert, Marieke Bruyne, Caroline Cauwenbergh, Hannah Verdin, et al. "Hidden Genetic Variation in LCA9-Associated Congenital Blindness Explained by 5′UTR Mutations and Copy-Number Variations of NMNAT1." Human Mutation 36, no. 12 (December 2015): 1188–96. https://doi.org/10.1002/humu.22899.

Daum, Janine M, Özkan Keles, Sjoerd JB Holwerda, Hubertus Kohler, Filippo M Rijli, Michael Stadler, and Botond Roska. "The Formation of the Light-Sensing Compartment of Cone Photoreceptors Coincides with a Transcriptional Switch." ELife 6 (November 6, 2017): e31437. https://doi.org/10.7554/eLife.31437.

Donovan, M, and T G Cotter. "Caspase-Independent Photoreceptor Apoptosis in Vivo and Differential Expression of Apoptotic Protease Activating Factor-1 and Caspase-3 during Retinal Development." Cell Death & Differentiation 9, no. 11 (November 2002): 1220–31. https://doi.org/10.1038/sj.cdd.4401105.

Donovan, Maryanne, Francesca Doonan, and Thomas G. Cotter. "Decreased Expression of Pro-Apoptotic Bcl-2 Family Members during Retinal Development and Differential Sensitivity to Cell Death." Developmental Biology 291, no. 1 (March 2006): 154–69. https://doi.org/10.1016/j.ydbio.2005.12.026.

Doonan, Francesca, Maryanne Donovan, and Thomas G. Cotter. "Caspase-Independent Photoreceptor Apoptosis in Mouse Models of Retinal Degeneration." The Journal of Neuroscience 23, no. 13 (July 2, 2003): 5723–31. https://doi.org/10.1523/JNEUROSCI.23-13-05723.2003.

Du, Jianhai, Haiwei Gu, Sally J Turner, Danijel Djukovic, Daniel Raftery, and James B Hurley. "Metabolite Profiles of Rod Photoreceptor Cell Death in Mouse Retinal Degeneration Models." Investigative Ophthalmology & Visual Science 55, no. 13 (April 30, 2014): 4374–4374.

Du, Jianhai, Jonathan D. Linton, and James B. Hurley. "Probing Metabolism in the Intact Retina Using Stable Isotope Tracers." In Methods in Enzymology, 561:149–70. Elsevier, 2015. https://doi.org/10.1016/bs.mie.2015.04.002.

968 Dvoriantchikova, Galina, Seemungal, Rajeev, and Dmitry Ivanov. "DNA Methylation Dynamics
969 During the Differentiation of Retinal Progenitor Cells Into Retinal Neurons Reveal a Role for the
970 DNA Demethylation Pathway." Frontiers in Molecular Neuroscience 12 (2019): 9.
971
972 Eblimit, Aiden, Smriti Agrawal Zaneveld, Wei Liu, Kandace Thomas, Keqing Wang, Yumei Li,
973 Graeme Mardon, and Rui Chen. "NMNAT1 E257K Variant, Associated with Leber Congenital
974 Amaurosis (LCA9), Causes a Mild Retinal Degeneration Phenotype." Experimental Eye
975 Research 173 (August 2018): 32–43. https://doi.org/10.1016/j.exer.2018.04.010.
976
977 Etingof, R N. "De Novo Biosynthesis of Purines in the Retina: Evolutionary Aspects" 37, no. 1
978 (2001): 10.
979
980 Falk, Marni J, Qi Zhang, Eiko Nakamaru-Ogiso, Chitra Kannabiran, Zoe Fonseca-Kelly,
981 Christina Chakarova, Isabelle Audo, et al. "NMNAT1 Mutations Cause Leber Congenital
982 Amaurosis." Nature Genetics 44, no. 9 (September 2012): 1040–45.
983 https://doi.org/10.1038/ng.2361.
984
985 Figley, Matthew D., Weixi Gu, Jeffrey D. Nanson, Yun Shi, Yo Sasaki, Katie Cunnea,
986 Alpeshkumar K. Malde, et al. "SARM1 Is a Metabolic Sensor Activated by an Increased
987 NMN/NAD+ Ratio to Trigger Axon Degeneration." Neuron, March 2021, S0896627321000830.
988 https://doi.org/10.1016/j.neuron.2021.02.009.
989
990 Finding of Rare Disease Genes (FORGE) Canada Consortium, Robert K Koenekoop, Hui Wang,
991 Jacek Majewski, Xia Wang, Irma Lopez, Huanan Ren, et al. "Mutations in NMNAT1 Cause
992 Leber Congenital Amaurosis and Identify a New Disease Pathway for Retinal Degeneration."
993 Nature Genetics 44, no. 9 (September 2012): 1035–39. https://doi.org/10.1038/ng.2356.
994
995 Furuta, Yasuhide, Oleg Lagutin, Brigid L M Hogan, and Guillermo C Oliver. "Retina- and
996 Ventral Forebrain-specific Cre Recombinase Activity in Transgenic Mice," n.d., 3.
997
998 Greenwald, Scott H, Emily E Brown, Michael J Scandura, Erin Hennessey, Raymond Farmer,
999 Jianhai Du, Yekai Wang, and Eric A Pierce. "Mutant NMNAT1 Leads to a Retina-Specific
1000 Decrease of NAD+ Accompanied by Increased Poly(ADP-Ribose) in a Mouse Model of
1001 NMNAT1 -Associated Retinal Degeneration." Human Molecular Genetics, March 11, 2021,
1002 ddab070. https://doi.org/10.1093/hmg/ddab070.
1003
1004 Greenwald, Scott H., Emily E. Brown, Michael J. Scandura, Erin Hennessey, Raymond Farmer,
1005 Basil S. Pawlyk, Ru Xiao, Luk H. Vandenberghe, and Eric A. Pierce. "Gene Therapy Preserves
1006 Retinal Structure and Function in a Mouse Model of NMNAT1-Associated Retinal
1007 Degeneration." Molecular Therapy - Methods & Clinical Development 18 (September 2020):
1008 582–94. https://doi.org/10.1016/j.omtm.2020.07.003.
1009
1010 Greenwald, Scott H., Jeremy R. Charette, Magdalena Staniszewska, Lan Ying Shi, Steve D.M.
1011 Brown, Lisa Stone, Qin Liu, et al. "Mouse Models of NMNAT1-Leber Congenital Amaurosis
1012 (LCA9) Recapitulate Key Features of the Human Disease." The American Journal of Pathology
1013 186, no. 7 (July 2016): 1925–38. https://doi.org/10.1016/j.ajpath.2016.03.013.

Gutierrez, Kimberley D., Michael A. Davis, Brian P. Daniels, Tayla M. Olsen, Pooja Ralli-Jain, Stephen W. G. Tait, Michael Gale, and Andrew Oberst. "MLKL Activation Triggers NLRP3-Mediated Processing and Release of IL-1β Independently of Gasdermin-D." The Journal of Immunology 198, no. 5 (March 1, 2017): 2156–64. https://doi.org/10.4049/jimmunol.1601757.

Houtkooper, Riekelt H., Carles Cantó, Ronald J. Wanders, and Johan Auwerx. "The Secret Life of NAD + : An Old Metabolite Controlling New Metabolic Signaling Pathways." Endocrine Reviews 31, no. 2 (April 2010): 194–223. https://doi.org/10.1210/er.2009-0026.

Kanow, Mark A, Michelle M Giarmarco, Connor SR Jankowski, Kristine Tsantilas, Abbi L Engel, Jianhai Du, Jonathan D Linton, et al. "Biochemical Adaptations of the Retina and Retinal Pigment Epithelium Support a Metabolic Ecosystem in the Vertebrate Eye." ELife 6 (September 13, 2017): e28899. https://doi.org/10.7554/eLife.28899.

Kayagaki, Nobuhiko, Bettina L. Lee, Irma B. Stowe, Opher S. Kornfeld, Karen O'Rourke, Kathleen M. Mirrashidi, Benjamin Haley, et al. "IRF2 Transcriptionally Induces GSDMD Expression for Pyroptosis." Science Signaling 12, no. 582 (May 21, 2019): eaax4917. https://doi.org/10.1126/scisignal.aax4917.

Kim, Daehwan, Ben Langmead, and Steven L Salzberg. "HISAT: A Fast Spliced Aligner with Low Memory Requirements." Nature Methods 12, no. 4 (April 2015): 357–60. https://doi.org/10.1038/nmeth.3317.

Kumaran, Neruban, Anthony T Moore, Richard G Weleber, and Michel Michaelides. "Leber Congenital Amaurosis/Early-Onset Severe Retinal Dystrophy: Clinical Features, Molecular Genetics and Therapeutic Interventions." British Journal of Ophthalmology 101, no. 9 (September 2017): 1147–54. https://doi.org/10.1136/bjophthalmol-2016-309975.

Kuribayashi, Hiroshi, Yukihiro Baba, Toshiro Iwagawa, Eisuke Arai, Akira Murakami, and Sumiko Watanabe. "Roles of Nmnat1 in the Survival of Retinal Progenitors through the Regulation of Pro-Apoptotic Gene Expression via Histone Acetylation." Cell Death & Disease 9, no. 9 (August 30, 2018). https://doi.org/10.1038/s41419-018-0907-0.

Lin, Jonathan B., Shunsuke Kubota, Norimitsu Ban, Mitsukuni Yoshida, Andrea Santeford, Abdoulaye Sene, Rei Nakamura, et al. "NAMPT-Mediated NAD + Biosynthesis Is Essential for Vision In Mice." Cell Reports 17, no. 1 (September 2016): 69–85. https://doi.org/10.1016/j.celrep.2016.08.073.

Love, Michael I, Wolfgang Huber, and Simon Anders. "Moderated Estimation of Fold Change and Dispersion for RNA-Seq Data with DESeq2." Genome Biology 15, no. 12 (December 2014): 550. https://doi.org/10.1186/s13059-014-0550-8.

Lundt, Samuel, Nannan Zhang, Jun-Liszt Li, Zhe Zhang, Li Zhang, Xiaowan Wang, Ruisi Bao, et al. "Metabolomic and Transcriptional Profiling Reveals Bioenergetic Stress and Activation of Cell Death and Inflammatory Pathways in Vivo after Neuronal Deletion of NAMPT." Journal of

Cerebral Blood Flow & Metabolism, February 9, 2021, 0271678X2199262. https://doi.org/10.1177/0271678X21992625.

McKenzie, Brienne A. "Fiery Cell Death: Pyroptosis in the Central Nervous System." Trends in Neurosciences, n.d., 19.

Miao, Edward A., Jayant V. Rajan, and Alan Aderem. "Caspase-1-Induced Pyroptotic Cell Death: Caspase-1-Induced Pyroptotic Cell Death." Immunological Reviews 243, no. 1 (September 2011): 206–14. https://doi.org/10.1111/j.1600-065X.2011.01044.x.

Mori, Valerio, Adolfo Amici, Francesca Mazzola, Michele Di Stefano, Laura Conforti, Giulio Magni, Silverio Ruggieri, Nadia Raffaelli, and Giuseppe Orsomando. "Metabolic Profiling of Alternative NAD Biosynthetic Routes in Mouse Tissues." Edited by Valerie de Crécy-Lagard. PLoS ONE 9, no. 11 (November 25, 2014): e113939. https://doi.org/10.1371/journal.pone.0113939.

Mukherjee, Piyali, Clayton W. Winkler, Katherine G. Taylor, Tyson A. Woods, Vinod Nair, Burhan A. Khan, and Karin E. Peterson. "SARM1, Not MyD88, Mediates TLR7/TLR9-Induced Apoptosis in Neurons." The Journal of Immunology 195, no. 10 (November 15, 2015): 4913–21. https://doi.org/10.4049/jimmunol.1500953.

Müller, Tammo, Christin Dewitz, Jessica Schmitz, Anna Sophia Schröder, Jan Hinrich Bräsen, Brent R. Stockwell, James M. Murphy, Ulrich Kunzendorf, and Stefan Krautwald. "Necroptosis and Ferroptosis Are Alternative Cell Death Pathways That Operate in Acute Kidney Failure." Cellular and Molecular Life Sciences 74, no. 19 (October 2017): 3631–45. https://doi.org/10.1007/s00018-017-2547-4.

Murakami, Y., H. Matsumoto, M. Roh, J. Suzuki, T. Hisatomi, Y. Ikeda, J. W. Miller, and D. G. Vavvas. "Receptor Interacting Protein Kinase Mediates Necrotic Cone but Not Rod Cell Death in a Mouse Model of Inherited Degeneration." Proceedings of the National Academy of Sciences 109, no. 36 (September 4, 2012): 14598–603. https://doi.org/10.1073/pnas.1206937109.

Nash, Benjamin M., Richard Symes, Himanshu Goel, Marcel E. Dinger, Bruce Bennetts, John R. Grigg, and Robyn V. Jamieson. "NMNAT1 Variants Cause Cone and Cone-Rod Dystrophy." European Journal of Human Genetics 26, no. 3 (March 2018): 428–33. https://doi.org/10.1038/s41431-017-0029-7.

Navas, Lola E., and Amancio Carnero. "NAD+ Metabolism, Stemness, the Immune Response, and Cancer." Signal Transduction and Targeted Therapy 6, no. 1 (December 2021): 2. https://doi.org/10.1038/s41392-020-00354-w.

Newton, K., D. L. Dugger, K. E. Wickliffe, N. Kapoor, M. C. de Almagro, D. Vucic, L. Komuves, et al. "Activity of Protein Kinase RIPK3 Determines Whether Cells Die by Necroptosis or Apoptosis." Science 343, no. 6177 (March 21, 2014): 1357–60. https://doi.org/10.1126/science.1249361.

1106 Ng, Soo Khai, John PM Wood, Glyn Chidlow, Guoge Han, Thaksaon Kittipassorn, Daniel J
1107 Peet, and Robert J Casson. "Cancer-like Metabolism of the Mammalian Retina: Mammalian
1108 Retina Metabolism." Clinical & Experimental Ophthalmology 43, no. 4 (May 2015): 367–76.
1109 https://doi.org/10.1111/ceo.12462.
1110
1111 Nikiforov, Andrey, Veronika Kulikova, and Mathias Ziegler. "The Human NAD Metabolome:
1112 Functions, Metabolism and Compartmentalization." Critical Reviews in Biochemistry and
1113 Molecular Biology 50, no. 4 (July 4, 2015): 284–97.
1114 https://doi.org/10.3109/10409238.2015.1028612.
1115
1116 Oakey, Lucy A., Rachel S. Fletcher, Yasir S. Elhassan, David M. Cartwright, Craig L. Doig,
1117 Antje Garten, Alpesh Thakker, et al. "Metabolic Tracing Reveals Novel Adaptations to Skeletal
1118 Muscle Cell Energy Production Pathways in Response to NAD + Depletion." Wellcome Open
1119 Research 3 (2018): 147. https://doi.org/10.12688/wellcomeopenres.14898.2.
1120
1121 Perrault, Isabelle, Sylvain Hanein, Xavier Zanlonghi, Valérie Serre, Michael Nicouleau, Sabine
1122 Defoort-Delhemmes, Nathalie Delphin, et al. "Mutations in NMNAT1 Cause Leber Congenital
1123 Amaurosis with Early-Onset Severe Macular and Optic Atrophy." Nature Genetics 44, no. 9
1124 (September 2012): 975–77. https://doi.org/10.1038/ng.2357.
1125
1126 Pertea, Mihaela, Daehwan Kim, Geo M Pertea, Jeffrey T Leek, and Steven L Salzberg.
1127 "Transcript-Level Expression Analysis of RNA-Seq Experiments with HISAT, StringTie and
1128 Ballgown." Nature Protocols 11, no. 9 (August 11, 2016): 1650–67.
1129 https://doi.org/10.1038/nprot.2016.095.
1130
1131 Pertea, Mihaela, Geo M Pertea, Corina M Antonescu, Tsung-Cheng Chang, Joshua T Mendell,
1132 and Steven L Salzberg. "StringTie Enables Improved Reconstruction of a Transcriptome from
1133 RNA-Seq Reads." Nature Biotechnology 33, no. 3 (March 2015): 290–95.
1134 https://doi.org/10.1038/nbt.3122.
1135
1136 Preyat, Nicolas, and Oberdan Leo. "Complex Role of Nicotinamide Adenine Dinucleotide in the
1137 Regulation of Programmed Cell Death Pathways." Biochemical Pharmacology 101 (February
1138 2016): 13–26. https://doi.org/10.1016/j.bcp.2015.08.110.
1139
1140 Raeisossadati, Reza, Merari F. R. Ferrari, Alexandre Hiroaki Kihara, Issam AlDiri, and Jeffrey
1141 M. Gross. "Epigenetic Regulation of Retinal Development." Epigenetics & Chromatin 14, no. 1
1142 (December 2021): 11. https://doi.org/10.1186/s13072-021-00384-w.
1143
1144 Rhee, K-D, J Yu, C Y Zhao, G Fan, and X-J Yang. "Dnmt1-Dependent DNA Methylation Is
1145 Essential for Photoreceptor Terminal Differentiation and Retinal Neuron Survival." Cell Death &
1146 Disease 3, no. 11 (November 2012): e427–e427. https://doi.org/10.1038/cddis.2012.165.
1147
1148 Sanman, Laura E, Yu Qian, Nicholas A Eisele, Tessie M Ng, Wouter A van der Linden, Denise
1149 M Monack, Eranthie Weerapana, and Matthew Bogyo. "Disruption of Glycolytic Flux Is a
1150 Signal for Inflammasome Signaling and Pyroptotic Cell Death." ELife 5 (March 24, 2016):
1151 e13663. https://doi.org/10.7554/eLife.13663.

Sasaki, Yo, Thomas M. Engber, Robert O. Hughes, Matthew D. Figley, Tong Wu, Todd Bosanac, Rajesh Devraj, Jeffrey Milbrandt, Raul Krauss, and Aaron DiAntonio. "CADPR Is a Gene Dosage-Sensitive Biomarker of SARM1 Activity in Healthy, Compromised, and Degenerating Axons." Experimental Neurology 329 (July 2020): 113252. https://doi.org/10.1016/j.expneurol.2020.113252.

Sasaki, Yo, Hiroki Kakita, Shunsuke Kubota, Abdoulaye Sene, Tae Jun Lee, Norimitsu Ban, Zhenyu Dong, et al. "SARM1 Depletion Rescues NMNAT1-Dependent Photoreceptor Cell Death and Retinal Degeneration." ELife 9 (October 27, 2020): e62027. https://doi.org/10.7554/eLife.62027.

Sasaki, Yo, Zachary Margolin, Benjamin Borgo, James J. Havranek, and Jeffrey Milbrandt. "Characterization of Leber Congenital Amaurosis-Associated NMNAT1 Mutants." Journal of Biological Chemistry 290, no. 28 (July 2015): 17228–38. https://doi.org/10.1074/jbc.M115.637850.

Sato, K., S. Li, W. C. Gordon, J. He, G. I. Liou, J. M. Hill, G. H. Travis, N. G. Bazan, and M. Jin. "Receptor Interacting Protein Kinase-Mediated Necrosis Contributes to Cone and Rod Photoreceptor Degeneration in the Retina Lacking Interphotoreceptor Retinoid-Binding Protein." Journal of Neuroscience 33, no. 44 (October 30, 2013): 17458–68. https://doi.org/10.1523/JNEUROSCI.1380-13.2013.

Seritrakul, Pawat, and Jeffrey M. Gross. "Tet-Mediated DNA Hydroxymethylation Regulates Retinal Neurogenesis by Modulating Cell-Extrinsic Signaling Pathways." Edited by Wolf Reik. PLOS Genetics 13, no. 9 (September 19, 2017): e1006987. https://doi.org/10.1371/journal.pgen.1006987.

Singh, Ratnesh K., Ramya K. Mallela, Abigail Hayes, Nicholas R. Dunham, Morgan E. Hedden, Raymond A. Enke, Robert N. Fariss, Hal Sternberg, Michael D. West, and Igor O. Nasonkin. "Dnmt1, Dnmt3a and Dnmt3b Cooperate in Photoreceptor and Outer Plexiform Layer Development in the Mammalian Retina." Experimental Eye Research 159 (June 2017): 132–46. https://doi.org/10.1016/j.exer.2016.11.014.

Sinha, Tirthankar, Jianhai Du, Mustafa S. Makia, James B. Hurley, Muna I. Naash, and Muayyad R. Al-Ubaidi. "Absence of Retbindin Blocks Glycolytic Flux, Disrupts Metabolic Homeostasis, and Leads to Photoreceptor Degeneration." Proceedings of the National Academy of Sciences 118, no. 6 (February 9, 2021): e2018956118. https://doi.org/10.1073/pnas.2018956118.

Song, Tanjing, Leixiang Yang, Neha Kabra, Lihong Chen, John Koomen, Eric B. Haura, and Jiandong Chen. "The NAD+ Synthesis Enzyme Nicotinamide Mononucleotide Adenylyltransferase (NMNAT1) Regulates Ribosomal RNA Transcription." Journal of Biological Chemistry 288, no. 29 (July 19, 2013): 20908–17. https://doi.org/10.1074/jbc.M113.470302.

Svoboda, Petr, Edita Krizova, Sarka Sestakova, Kamila Vapenkova, Zdenek Knejzlik, Silvie Rimpelova, Diana Rayova, et al. "Nuclear Transport of Nicotinamide Phosphoribosyltransferase Is Cell Cycle–Dependent in Mammalian Cells, and Its Inhibition Slows Cell Growth." Journal of Biological Chemistry 294, no. 22 (May 2019): 8676–89. https://doi.org/10.1074/jbc.RA118.003505.

Swanson, Karen V., Meng Deng, and Jenny P.-Y. Ting. "The NLRP3 Inflammasome: Molecular Activation and Regulation to Therapeutics." Nature Reviews Immunology 19, no. 8 (August 2019): 477–89. https://doi.org/10.1038/s41577-019-0165-0.

Swaroop, Anand, Douglas Kim, and Douglas Forrest. "Transcriptional Regulation of Photoreceptor Development and Homeostasis in the Mammalian Retina." Nature Reviews Neuroscience 11, no. 8 (August 2010): 563–76. https://doi.org/10.1038/nrn2880.

Vandenabeele, Peter, Lorenzo Galluzzi, Tom Vanden Berghe, and Guido Kroemer. "Molecular Mechanisms of Necroptosis: An Ordered Cellular Explosion." Nature Reviews Molecular Cell Biology 11, no. 10 (October 2010): 700–714. https://doi.org/10.1038/nrm2970.

Wang, Xiaolin, Yu Fang, Rongsheng Liao, and Tao Wang. "Targeted Deletion of Nmnat1 in Mouse Retina Leads to Early Severe Retinal Dystrophy." Preprint. Developmental Biology, October 29, 2017. https://doi.org/10.1101/210757.

Zhang, Rui, Weiyong Shen, Jianhai Du, and Mark C. Gillies. "Selective Knockdown of Hexokinase 2 in Rods Leads to Age-Related Photoreceptor Degeneration and Retinal Metabolic Remodeling." Cell Death & Disease 11, no. 10 (October 2020): 885. https://doi.org/10.1038/s41419-020-03103-7.

Zhang, Tong, Jhoanna G. Berrocal, Jie Yao, Michelle E. DuMond, Raga Krishnakumar, Donald D. Ruhl, Keun Woo Ryu, Matthew J. Gamble, and W. Lee Kraus. "Regulation of Poly(ADP-Ribose) Polymerase-1-Dependent Gene Expression through Promoter-Directed Recruitment of a Nuclear NAD+ Synthase*." Journal of Biological Chemistry 287, no. 15 (April 2012): 12405–16. https://doi.org/10.1074/jbc.M111.304469.

Zhao, Zhi Ying, Xu Jie Xie, Wan Hua Li, Jun Liu, Zhe Chen, Ben Zhang, Ting Li, et al. "A Cell-Permeant Mimetic of NMN Activates SARM1 to Produce Cyclic ADP-Ribose and Induce Non-Apoptotic Cell Death." IScience 15 (May 31, 2019): 452–66. https://doi.org/10.1016/j.isci.2019.05.001.

Zhu, Siyan, Michelle Yam, Yekai Wang, Jonathan D. Linton, Allison Grenell, James B. Hurley, and Jianhai Du. "Impact of Euthanasia, Dissection and Postmortem Delay on Metabolic Profile in Mouse Retina and RPE/Choroid." Experimental Eye Research 174 (September 2018): 113–20. https://doi.org/10.1016/j.exer.2018.05.032.